

© Copyright by Linda Quon 2014

All Rights Reserved

**PHYSICAL-MODEL SIMULATIONS OF SPILLS OF ETHANOL- AND
METHANOL-BLENDED FUELS AND PORE WATER IMPACTS**

A Thesis

Presented to

the Faculty of the Department of Civil and Environmental Engineering

University of Houston

In Partial Fulfillment

of the Requirements for the Degree

Master of Science

in Environmental Engineering

by

Linda L. Quon

August 2014

**PHYSICAL-MODEL SIMULATIONS OF SPILLS OF ETHANOL- AND
METHANOL-BLENDED FUELS AND PORE WATER IMPACTS**

Linda L. Quon

Approved:

Chair of the Committee
William G. Rixey,
Associate Professor,
Civil and Environmental Engineering

Committee Members:

Shankar Chellam,
Professor,
Civil and Environmental Engineering

Cumaraswamy Vipulanandan,
Professor,
Civil and Environmental Engineering

Suresh K. Khator,
Associate Dean,
Cullen College of Engineering

Hanadi S. Rifai,
Professor, and
Director of the Environmental
Engineering Graduate Program

ACKNOWLEDGEMENTS

I am deeply grateful to all of the people who have made this work possible. I would like to first thank my advisor Dr. William Rixey for his patience, guidance, and generosity in support of this project and thesis. I would also like to thank the members of my committee, Dr. Shankar Chellam and Dr. Cumaraswamy Vipulanandan for giving their time and input.

I am fortunate to share the lab with people who make it an enjoyable place to come to work. My fellow group members Irina Mamonkina, Ali Mirnami, Rishi Saladi and Yi Zhang have each provided invaluable help throughout this process.

Finally, I would like to thank my friends and family for their continuing support and encouragement.

**PHYSICAL-MODEL SIMULATIONS OF SPILLS OF ETHANOL- AND
METHANOL-BLENDED FUELS AND PORE WATER IMPACTS**

An Abstract

of a

Thesis

Presented to

the Faculty of the Department of Civil and Environmental Engineering

University of Houston

In Partial Fulfillment

of the Requirements for the Degree

Master of Science

in Environmental Engineering

by

Linda L. Quon

August 2014

ABSTRACT

To assess source formation, phase separation, capillary zone depression, alcohol transport and potential pore-water impacts, unsaturated zone releases of ethanol- and methanol-blended fuels were compared in two-dimensional continuous flow experiments. Experiments were conducted with blends of varying alcohol content (15, 25, 50 and 85 vol. %).

Visualization and image analysis of the releases showed decreases in residual NAPL saturation and increases in area impacted by NAPL with increasing alcohol content for blends of both alcohols. Comparing equivalent alcohol-content fuels, spill areas were less for the methanol blends than for the corresponding ethanol blends while residual saturations were greater for the methanol blends.

Aqueous methanol and hydrocarbon concentrations were measured downstream of an M15 release and compared with a source dissolution and transport model. Source depletion of hydrocarbons was significantly faster than that predicted for equilibrium dissolution of the NAPL, suggesting flow bypassing of a portion of the NAPL source.

TABLE OF CONTENTS

ACKNOWLEDGEMENTS	v
ABSTRACT	vii
TABLE OF CONTENTS	viii
LIST OF FIGURES	xi
LIST OF TABLES	xiv
CHAPTER 1: Introduction	1
1.1 Background	1
1.1.1 Oxygenate Usage in Transportation Gasolines.....	1
1.1.2 Source and Production of Ethanol and Methanol	2
1.1.3 Blended Fuel Releases in the Environment	2
1.2 Properties of Alcohol-Blended Fuels	3
1.2.1 Physical and Chemical Properties of Ethanol and Methanol.....	3
1.2.2 Cosolvency Effects	3
1.3 Research Objectives	6
1.4 Thesis Organization.....	6
CHAPTER 2: Literature Review	7
2.1 Introduction	7
2.2 Effects of Methanol on Fuel Behavior	7
2.2.1 Equilibrium Batch Experiments.....	7
2.2.2 Saturated-Flow Column Studies	7
2.2.3 Field Scale Studies	8
2.3 Effects of Ethanol on Fuel Behavior	9
2.3.1 Equilibrium Batch Experiments.....	9
2.3.2 Saturated-Flow Column Studies	9

2.3.3 Bench Scale Studies	10
2.3.4 Pilot and Field Scale Studies.....	11
2.4 Knowledge Gaps	12
CHAPTER 3: Experimental Overview.....	13
3.1 Experimental Methods	13
3.1.1 Experimental Setup.....	13
3.1.2 Cell Hydraulics	17
3.1.3 Blended Fuels.....	18
3.1.4 Dyes and Tracers.....	20
3.1.5 Methods of Analysis	20
CHAPTER 4: Results and Discussion.....	22
4.1 Methanol Blend Releases	22
4.1.1 M15 Release.....	22
4.1.2 M25 Release.....	23
4.1.3 M50 Release.....	23
4.1.4 M85 Release.....	25
4.1.5 Summary of Methanol Blend Releases	26
4.2 Duplicate Ethanol Blend Releases	27
4.2.1 Results.....	27
4.3 Comparison of Methanol and Ethanol Releases.....	30
4.4 75-mL M15 Release and Porewater Measurements	35
4.4.1 Visualization Study	35
4.4.2 Pore-water Concentration Measurements	35
4.4.3 Pore-water Concentration Modeling.....	41
4.4.3.1 Plume Transport Model	41
4.4.3.2 Theoretical Source Parameter Calculations	44
4.4.3.3 Modeling Results and Analysis.....	47

CHAPTER 5: Source Modeling	49
5.1 Advection-Diffusion Equation	49
5.2 Continuous Source Parameters.....	49
5.3 Continuous Source Solutions	51
5.3.1 Point Source Solutions.....	51
5.3.2 Gaussian Source Solution	54
5.3.3 Finite Line Source Solution	56
5.3.4 Comparison of Continuous Source Models	58
CHAPTER 6: Conclusions and Future Work	60
6.1 Blended Fuel Releases.....	60
6.2 Pore Water Impacts	61
6.3 Source Modeling	62
6.4 Recommendations for Future Work	62
REFERENCES	64
APPENDIX A: Methanol Release Visualization – Additional Data	69
APPENDIX B: 75-ML M15 Release Porewater Measurements	75
APPENDIX C: Capillary Pressure-Water Saturation Measurements	79

LIST OF FIGURES

Figure 1-1. Simulated ternary phase diagrams at 25 ⁰ C for (a) ethanol-benzene-water system (b) methanol-benzene-water system (Lee 2008).	4
Figure 3-1. 2D continuous-flow cell used for release visualization.	14
Figure 3-2. Diagram of injection and sampling ports and tracer study.....	16
Figure 3-3. Layout of bench-scale cells used in (a) ethanol-blended fuel experiments and (b) methanol-blended fuel experiments.	17
Figure 3-4. Visualization of propylene glycol tracer (a) immediately after injection, (b) 24 hours after injection and (c) 48 hours after injection.	20
Figure 4-1. Visualization of M15 release in the capillary zone (a) after injection, (b) 24 hours after injection, and (c) one week after injection.....	22
Figure 4-2. Visualization of M25 release in the capillary zone (a) after injection, (b) 24 hours after injection, and (c) one week after injection.....	23
Figure 4-3. Visualization of M50 release in the capillary zone (a) after injection, (b) 24 hours after injection, and (c) one week after injection.....	24
Figure 4-4. Visualization of M85 release in the capillary zone (a) after injection, (b) 24 hours after injection, and (c) one week after injection.....	25
Figure 4-5. NAPL saturation and pore volume impacted by NAPL for 30-mL methanol fuel blend releases.	27
Figure 4-6. Duplicate visualization experiments of ethanol-blended fuel releases	28
Figure 4-7. NAPL saturations and contaminated pore volumes for initial and duplicate ethanol-blended fuel releases	29
Figure 4-8. Visual comparison of (a) 20-mL E15 and (b) 30-mL M15 releases.	31

Figure 4-9. Visual comparison of (a) 20-mL E25 and (b) 30-mL M25 releases.	31
Figure 4-10. Visual comparison of (a) 20-mL E50 and (b) 30-mL M50 releases.	32
Figure 4-11. Visual comparison of (a) 20-mL E85 and (b) 30-mL M85 releases.	32
Figure 4-12. Final saturations and normalized spill areas for alcohol blended fuels.....	34
Figure 4-13. Visualization of 75-mL M15 release in the capillary zone (a) after injection, (b) 24 hours after injection, and (c) one week after injection.	35
Figure 4-14. Port 1 measured hydrocarbon and methanol concentrations and model (Equations 4-6 and 4-1) values.	36
Figure 4-15. Port 2 measured hydrocarbon and methanol concentrations and model (Equations 4-6 and 4-1) values.	37
Figure 4-16. Port 4 measured hydrocarbon and methanol concentrations.....	38
Figure 4-17. Methanol measured concentrations and model curves (Equation 4-1) at (a) Port 1 and (b) Port 2.....	38
Figure 4-18. Benzene measured concentrations and model curves (Equation 4-6) at (a) Port 1 and (b) Port 2.....	39
Figure 4-19. Toluene measured concentrations and model curves (Equation 4-6) at (a) Port 1 and (b) Port 2.....	39
Figure 4-20. m-Xylene measured concentrations and model curves (Equation 4-6) at (a) Port 1 and (b) Port 2.....	40
Figure 4-21. 1,2,4-TMB measured concentrations and model curves (Equation 4-6) at (a) Port 1 and (b) Port 2.....	40
Figure 4-22. Plume transport model scenario.	42

Figure 5-1. Transient point source solution (Eq. 5-6) dimensionless concentrations C/C_0 after one week.	52
Figure 5-2. Steady-state point source solution (Eq. 5-7) dimensionless concentrations C/C_0	52
Figure 5-3. Dimensionless centerline concentrations downstream of a point source at various times (Eq. 5-6).....	53
Figure 5-4. Dimensionless centerline concentrations downstream of a point source for transient ($t=7$ days) and steady-state (Eq. 5-7) conditions.....	53
Figure 5-5. Dimensionless concentrations C/C_0 downstream of a continuous Gaussian source ($\sigma = 2.5$ cm) after one week.	56
Figure 5-6. Dimensionless centerline concentration profiles downstream of a continuous Gaussian source ($\sigma = 2.5$ cm) at various times.	56
Figure 5-7. Steady-state dimensionless concentrations	57
Figure 5-8. Steady-state concentration profiles downstream of a finite line source of width $b = 10$ cm.	57
Figure 5-9. Steady-state centerline concentration profiles for Gaussian, finite line, and point sources.	58

LIST OF TABLES

Table 1-1. Physical and chemical properties of ethanol and methanol.....	4
Table 3-1. Properties of Ottawa Federal-Fine Sand.....	14
Table 3-2. 2D Cell Characteristics.....	18
Table 3-3. Physical-chemical properties of alcohols and LNAPL hydrocarbon components.....	19
Table 4-1. NAPL saturations and pore volume impacted by NAPL for 30-mL methanol fuel blend releases.....	26
Table 4-2. NAPL saturations and contaminated pore volumes for initial and duplicate ethanol-blended fuel releases.....	30
Table 4-3. Final saturations and normalized spill areas for alcohol blended fuels.....	34
Table 4-4. Theoretical calculated parameters.....	47
Table 4-5. Model fitted parameters.....	48
Table 5-1. Continuous source parameters.....	50
Table 5-2. Point source solution parameters.....	51
Table 5-3. Gaussian source solution parameters.....	55

CHAPTER 1: INTRODUCTION

1.1 Background

1.1.1 Oxygenate Usage in Transportation Gasolines

As part of the Clean Air Act Amendments of 1990 (CAAA), the use of reformulated gasoline (RFG) was mandated in areas across the United States to improve air quality via reduced vehicle emissions. With this legislation, compositional specifications for RFG were introduced which included a minimum oxygen content of 2.0 weight percent. The oxygenate methyl tertiary-butyl ether (MTBE) was first used to meet the oxygen requirement but was later supplanted due to groundwater contamination and toxicity concerns.

The Energy Policy Act of 2005 (EPAAct) eliminated the RFG oxygenate requirement and established the Renewable Fuel Standard (RFS) which called for continuing increases in the amount of renewable fuel used in gasoline. Bolstered by state subsidies and incentives, this renewable fuel requirement has largely been fulfilled by the use of ethanol (U.S. Department of Agriculture, 2007).

Domestically, ethanol is most commonly found in the fuel blends E10 (10% v/v ethanol) and E95 (95% v/v ethanol), used for direct vehicle fueling and the mixing of other ethanol-blended fuels, respectively. In Brazil, intermediate ethanol blends (E20 and E25) have been in use for several decades (Freitas and Barker 2011).

The oxygenate methanol initially gained broad recognition as a viable transportation fuel in the 1970s (Reed 1973). Thereafter, several vehicles were developed for use with high methanol content blends such as M85 (85% v/v methanol). In the 1990s, dedicated fleets of vehicles utilizing these methanol blends were operated in

California and New York State. Nevertheless, methanol blended fuels failed to gain traction in the marketplace due to the falling price of petroleum at the time and a lack of advocacy for their use (Bromberg 2010). Recently, however, there has been renewed interest in methanol as a renewable fuel component due to the diversity and availability of potential feedstocks. Methanol blends are in wider use abroad, with a broad range of fuels from M5 to M100 available across China, the world's largest methanol producer (Yang and Jackson 2012).

1.1.2 Source and Production of Ethanol and Methanol

Ethanol is primarily produced through the fermentation of sugar- or starch-based feedstocks, though cellulosic feedstocks can also be used. In the United States, corn is used as the leading source.

For economic reasons, methanol is chiefly produced domestically from a natural gas feedstock. Through steam-reforming, this natural gas is converted into a synthesis gas. The synthesis gas, consisting of CO, CO₂, and hydrogen, then reacts over a catalyst to form methanol. However, methanol can also be produced from many other feedstocks including coal and many renewable sources.

1.1.3 Blended Fuel Releases in the Environment

With corn as the principal feedstock used in ethanol manufacture in the United States, ethanol production plants are concentrated in the Corn Belt, a region encompassing several Midwestern states where the majority of domestic corn is grown. Ethanol produced in these plants is then transported via rail, truck or pipeline to the coastlines where great demand exists. Manufactured methanol is transported by similar

means, though production is less centralized due to the geographic spread of current natural gas supplies.

In the course of the overland transit required to deliver the fuels to consumers, accidents may occur that can result in fuel infiltrating the subsurface. Moreover, in addition to potential releases during transport, fuels can also enter the subsurface via leaking storage tanks as well as spills at distribution terminals (ITRC 2011, Powers 2001).

1.2 Properties of Alcohol-Blended Fuels

1.2.1 Physical and Chemical Properties of Ethanol and Methanol

Ethanol and methanol are primary alcohols whose physical and chemical properties (Table 1-1) influence the behavior of the blended fuels that contain them. Both alcohols are buoyant, with similar specific gravities much less than that of water. Both alcohols are also hygroscopic, having an affinity for water and water vapor, as well as being completely miscible in water. Further, Henry's Law constants for ethanol and methanol are low, such that volatilization from the aqueous phase is unlikely.

1.2.2 Cosolvency Effects

In contrast to the hydrophobic hydrocarbons found in gasoline, ethanol and methanol are cosolvents, miscible in both the water and NAPL phases. As a result, these alcohols can induce a cosolvency effect in which their presence facilitates greater aqueous solubility of the NAPL. This behavior in cosolvent systems is depicted in ternary phase diagrams.

Table 1-1. Physical and chemical properties of ethanol and methanol.

Property	Ethanol	Methanol
Chemical formula	C ₂ H ₅ OH	CH ₃ OH
Molecular weight	46.07 ⁽¹⁾	32.04 ⁽¹⁾
Specific gravity, 15° C [g/cm ³]	0.789 ⁽¹⁾	0.791 ⁽¹⁾
Boiling point [°C]	78.24 ⁽¹⁾	64.5 ⁽¹⁾
Melting point [°C]	-114.14 ⁽¹⁾	-97.5 ⁽¹⁾
Vapor pressure, 25°C [mm Hg]	59.26 ⁽³⁾	127 ⁽³⁾
Water solubility [mg/L]	miscible	Miscible
Viscosity, 25°C [cp]	1.074 ⁽¹⁾	0.544 ⁽¹⁾
Surface tension [mN/m]	21.82 ⁽¹⁾	22.51 ⁽¹⁾
Henry's Law Constant, 25°C		
[atm-L/mole]	0.00507 ⁽³⁾	0.00455 ⁽³⁾
Dimensionless	2.57 x 10 ⁻⁴ ⁽⁴⁾	1.09 x 10 ⁻⁴ ⁽⁵⁾
Diffusivity (aq.), 25°C [cm ² /sec]	1.22 x 10 ⁻⁵ ⁽⁶⁾	1.54 x 10 ⁻⁵ ⁽⁶⁾
Log Kow	0.20 ⁽²⁾	0.71 ⁽²⁾

⁽¹⁾Lide, 2013

⁽²⁾Sangster, 1989

⁽³⁾Gaffney et al., 1987

⁽⁴⁾US EPA, 1998

⁽⁵⁾Merck Index, 2006

⁽⁶⁾Hao and Leaist, 1996

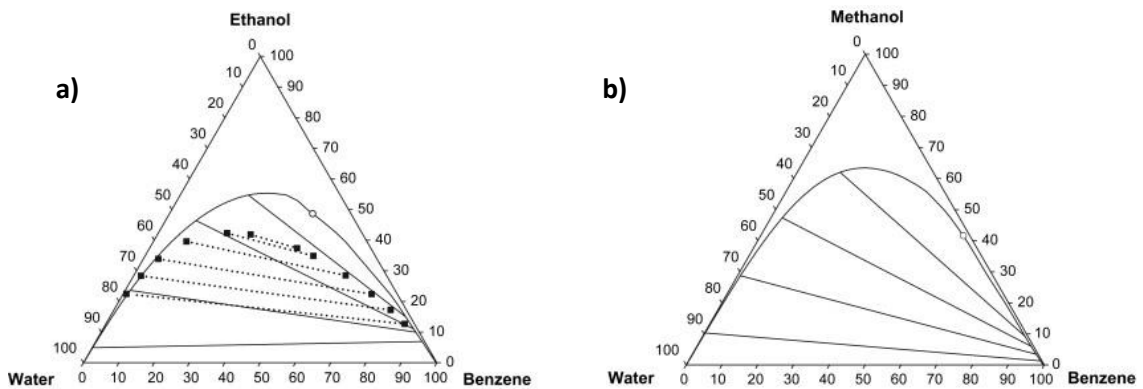


Figure 1-1. Simulated ternary phase diagrams at 25°C for (a) ethanol-benzene-water system (b) methanol-benzene-water system (Lee 2008).

The partitioning behavior of three-component NAPL-cosolvent-water systems containing ethanol or methanol as a cosolvent is similar (Figure 1-1). In both cosolvent systems, the two-phase region of the phase diagram is characterized by tie lines having negative slope, demonstrating the inclination of the cosolvents to preferentially partition into the aqueous phase. However, the area of the two-phase region is greater for the methanol system than for ethanol, indicating a greater percentage of mixture combinations that will result in two-phase systems.

Surface and interfacial tension (IFT) are also affected by the presence of cosolvents. IFT at the plait point is zero, as the compositions of the two existing phases are identical. As the mixture moves away from the plait point, compositional changes in the fluid phases alter the surface tension and IFT.

As ethanol partitions into the aqueous phase of a three-component system, surface tension is progressively decreased with increasing ethanol (McDowell and Powers 2003). IFT is likewise reduced with rising aqueous ethanol concentrations in similar systems for iso-octane as well as gasolines (retail and simulated).

Changes in fluid viscosity are similarly related to the partitioning behavior. Ethanol (1.074 cp) is more viscous than water (0.890 cp) at 25 °C, while methanol (0.544 cp) is less viscous. However, as water is added to a three-component system, viscosity of the mixture increases throughout the single-phase region. In the two-phase region, the viscosity of the aqueous phase increases significantly to almost three times the viscosity of the two-component NAPL-cosolvent system before decreasing at total system water contents >70% (Lee and Ha 2012).

1.3 Research Objectives

This study investigated ethanol- and methanol-blended fuel releases in the capillary zone. Experiments were performed at the bench scale using fuels with compositions varying from 15 to 85 % v/v alcohol in order to

- (1) Evaluate the qualitative and quantitative effects of fuel composition on NAPL source zone formation, mobilization and redistribution as well as alcohol transport
- (2) Compare the behavior of ethanol- and methanol-blended fuel releases
- (3) Assess potential pore-water impacts of blended-fuel releases.

In this work, only physical-chemical effects were considered; microbial effects were not taken into account.

1.4 Thesis Organization

Background information regarding the properties and typical applications of alcohol-blended fuels is presented in Chapter 1 along with the objectives of this work. Next, relevant literature concerning releases of ethanol- and methanol-blended fuels is reviewed in Chapter 2. Experimental setup and methods are then described in Chapter 3 with results and discussion provided in Chapter 4. Chapter 5 examines source models derived from the advection-diffusion equation. Finally, conclusions from this work and suggestions for future work are presented in Chapter 6.

CHAPTER 2: LITERATURE REVIEW

2.1 Introduction

The behavior of oxygenated fuels has been investigated in previous studies in batch experiments and at the lab, pilot and field scales. These studies have focused on high and low alcohol content fuels, primarily the E10 and E95 ethanol blends and the methanol blend M85.

2.2 Effects of Methanol on Fuel Behavior

2.2.1 Equilibrium Batch Experiments

Equilibrium batch experiments were performed by Poulsen et al. (1992) with methanol-blended fuels of varying methanol content. At a 10:1 aqueous phase to fuel ratio, aqueous concentrations of the BTEX compounds, with the exception of benzene, remained constant for methanol blends up to 90% methanol, suggesting that BTEX solubility was not enhanced at low methanol concentrations. At a 1:1 aqueous-phase to benzene ratio, aqueous benzene concentrations increased linearly with increasing methanol content up to 20-30% methanol content, beyond which, the concentrations exhibited logarithmic behavior.

2.2.2 Saturated-Flow Column Studies

Using blends of methanol and the conventional gasoline API PS-6 in saturated flow column experiments, releases of M85 yielded almost complete (greater than 90%) recovery of methanol (Barker et al. 1992, Donaldson et al. 1993). However, hydrocarbon recovery from these releases was limited. Barker et al. (1992) recorded benzene recovery at 78% with xylenes recovery at 20%; Donaldson et al. (1993) observed similar benzene recovery with 45% recovery of toluene. This recovery of benzene and toluene from the

M85 releases was much greater than from the M0 control releases in which hydrocarbon recovery was less than 10%. From this reduced recovery of hydrocarbons, the presence of a gasoline residual remaining in the column was inferred (Barker et al. 1992).

Maximum effluent concentrations of BTEX compounds observed in M85 column experiments were greater than BTEX concentrations measured in an M0 release (Rixey and Dortch 1992) and those expected from an M0 release based on component solubility (Donaldson et al. 1993). Based on the breakthrough curves of the effluent concentrations, Donaldson et al. (1993) reported a delay in reaching maximum BTEX concentrations after methanol concentrations had peaked. In the subsequent tailing following the peak concentrations, BTEX concentrations were in line with values expected from a pure gasoline phase (Barker et al. 1992, Donaldson et al. 1993). Additionally, released M85 generated a residual gasoline source along the entire column length, though concentrated near the inlet injection site (Donaldson et al. 1993). In contrast, the pure PS-6 gasoline generated a residual spanning only the first 5 cm of the 12.5 cm long column.

2.2.3 Field Scale Studies

A field scale test was conducted at the Canadian Forces Base in Borden, Ontario in which one slug of M85 was injected below the water table alongside PS-6 gasoline and chloride, used as a conservative tracer (Barker et al. 1992, Barker et al. 1993). In this test, methanol migrated at the same rate as the groundwater, with far greater longitudinal than transverse dispersion. Methanol was not present in sufficient quantities to affect the migration of the BTEX compounds.

2.3 Effects of Ethanol on Fuel Behavior

2.3.1 Equilibrium Batch Experiments

Similar to methanol, batch partitioning experiments were performed for NAPL-water systems with ethanol as a cosolvent (He et al. 2011, Heermann and Powers 1998, Rixey et al. 2005). Analogous to methanol, increasing aqueous-phase ethanol concentrations resulted in logarithmic increases in cosolvency of xylene and the other BTEX compounds for aqueous ethanol volume fractions greater than 0.20 (Heermann and Powers 1998). Additionally, cosolvency was inversely related to the solubility and hydrophobicity of the hydrocarbon compounds. The most soluble hydrocarbon component, benzene, exhibited the lowest concentration enhancement (He et al. 2011, Rixey et al. 2005) while xylene, the most hydrophobic compound, showed the greatest increase in partition coefficient (Heermann and Powers 1998).

2.3.2 Saturated-Flow Column Studies

A series of experiments by Rixey et al. (2005) explored three fuel release scenarios involving ethanol in saturated flow columns. Effluent BTEX concentrations were raised slightly as a result of emplaced gasohol (E15), limited by the low amount of ethanol present in the fuel. However, a pulse of neat ethanol released on emplaced fuel (E0) produced substantial increases in aqueous BTEX concentrations in the effluent, though concentrations were restricted by the depletion of the BTEX compounds and were dependent upon the amount of contact between ethanol and the emplaced NAPL. A pulse release of E95 generated a residual within the column, providing a long-term source of BTEX, similar to the emplaced gasohol.

2.3.3 Bench Scale Studies

The behavior of ethanol and fuels was also investigated at the bench scale in two-dimensional studies that allowed for clear visualization of releases (Capiro et al. 2007, McDowell and Powers 2003, McDowell et al. 2003, Stafford et al. 2009).

In an injection of low ethanol content E10 near the surface, McDowell and Powers (2003) observed the rapid accumulation of ethanol in the unsaturated zone, partitioned into the aqueous phase. The gasoline phase continued to migrate downwards and pooled at the capillary fringe, where it spread laterally, mostly depleted of ethanol. In comparing this E10 release to one of pure gasoline (E0), the authors noted that the ethanol had no noticeable effect on the size, shape or saturation of the gasoline residual.

A release of E95 at the water table migrated upwards through the capillary fringe due to buoyancy and an interfacial tension gradient (Capiro et al. 2007). Ethanol again phase-separated in the capillary zone, thus lowering the surface tension of the aqueous phase and resulting in significant depression of the capillary fringe. This fuel behavior was unlike that of a similar injection of unoxygenated NAPL, which did not migrate upwards. It remained pooled at the water table instead.

In cases of ethanol released onto existing NAPL, NAPL was dissolved and mobilized ahead of the advancing ethanol front. For a surface ethanol injection with a pool of residual NAPL located at the capillary fringe, NAPL moved downwards in front of the migrating ethanol, increasing the concentration of NAPL at the capillary fringe (McDowell et al. 2003). The lowered capillary fringe resulting from the presence of ethanol produced further increases in the concentration of the NAPL pool as surrounding NAPL drained into the depression.

For an ethanol release near the top of the capillary fringe upstream of a vertical source spanning the saturated and unsaturated zones, ethanol traveled horizontally, generating lenses of NAPL above and below the path of the ethanol (Stafford et al. 2009). The capillary fringe height was lowered due to the amount of ethanol present, though it began to recover as the ethanol was flushed from the system.

2.3.4 Pilot and Field Scale Studies

The results of ethanol fuel releases conducted at the pilot and field scales have largely corroborated results from smaller bench scale studies. In pilot scale releases of E95 (Capiro et al. 2007) and neat ethanol on emplaced NAPL (Stafford et al. 2009), ethanol and hydrocarbons were transported above the water table, with ethanol flow driven by buoyancy and interfacial tension gradients. However, ethanol transport in the capillary fringe in this scale aquifer was retarded in comparison with a saturated zone bromide tracer (Capiro et al. 2007).

In an E10 release at the Canadian Forces Base Borden, Freitas and Barker (2011) observed that most of the ethanol was retained in the unsaturated zone above the capillary fringe. The retained ethanol remained at a depth close to that of the release and was unaffected by fluctuations in the height of the water table. This partitioning of the ethanol into the aqueous phase had the additional effect of separating the ethanol from the NAPL phase, limiting solubility enhancement and reductions in hydrocarbon biodegradation (Freitas et al. 2011).

One year following the aforementioned E10 release, an E95 release at the same site simulated a denatured ethanol release on a gasoline residual (Freitas and Barker 2013). The larger volume of ethanol in this E95 spill allowed ethanol to reach the

capillary fringe and spread laterally. The greater amount of ethanol partitioning to the aqueous phase caused significant depression of the capillary fringe as well as accumulation of NAPL beneath the areas with high ethanol concentrations.

2.4 Knowledge Gaps

Previous studies of alcohol-blended fuels have focused on high- or low-alcohol-content blends with 10, 15, 85 or 95 volume % alcohol, with recent work examining the intermediate ethanol fuel blends E25 and E50 (Mamonkina 2011). The behavior of equivalent intermediate methanol blends is unknown, however.

Though similar, ethanol and methanol are differentiated in several key aspects, including varying aqueous surface tensions, partitioning behavior and cosolvency. This work investigates the impact of differences in the behavior of these two alcohols with respect to spills in the subsurface unsaturated zone.

CHAPTER 3: EXPERIMENTAL OVERVIEW

Methanol and ethanol fuel blends were injected into the capillary zones of continuous-flow 2D cells. The behavior of these releases was recorded and analyzed from the time of injection up to one week following injection.

Examining the blends M15, M25, M50 and M85, four original methanol-blended fuel injections were conducted during which visualization data was collected. Likewise, duplicates of four previous single experiments (Mamonkina 2011) injecting the ethanol-blended fuels E15, E25, E50 and E85 were performed. The ethanol blends tested in these duplicate experiments matched the alcohol/NAPL volume compositions of the corresponding methanol blends.

In addition to these shorter-term weeklong experiments, a larger 75-mL M15 fuel injection was conducted. Visualization data was obtained in this experiment as well as pore-water concentration measurements, which were taken for 50 days following the release.

3.1 Experimental Methods

3.1.1 Experimental Setup

Experimental conditions and materials for the releases were chosen to mimic as closely as possible the conditions of the initial ethanol-blended fuel experiments from previous work (Mamonkina 2011). These analogous conditions allowed for reasonable comparisons between the initial and duplicate ethanol blend releases and between the ethanol and methanol blend releases.

The release experiments were performed in similar bench scale continuous-flow 2D cells (Figure 3-1). The methanol blend releases were conducted in a larger (50 cm x

55 cm x 1.5 cm) cell with a glass front wall and an acrylic back wall. The duplicate ethanol blend releases were conducted in a smaller (40 cm x 45 cm x 1 cm) glass-walled cell to match the conditions of the initial experiments.

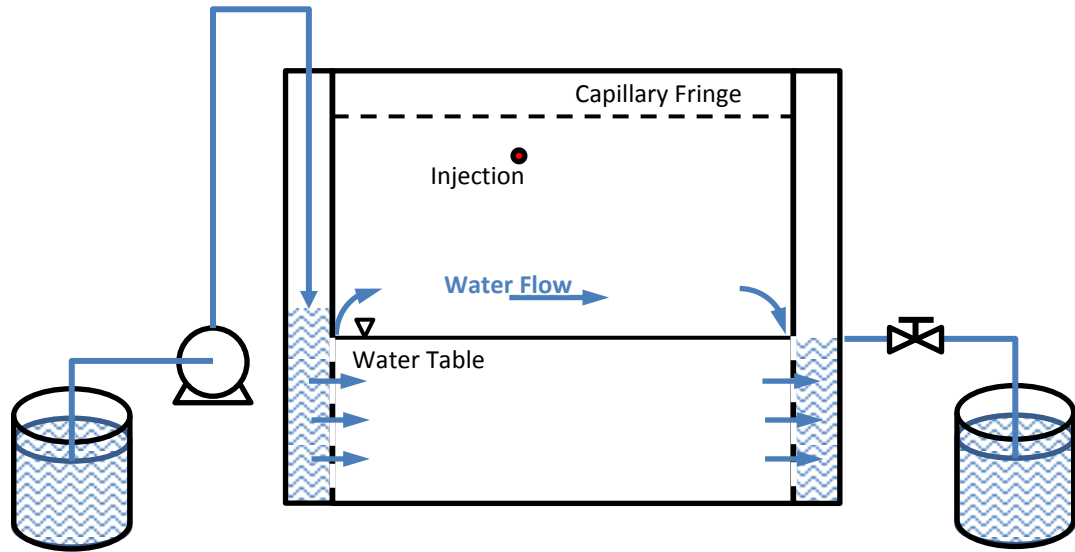


Figure 3-1. 2D continuous-flow cell used for release visualization.

Ottawa Federal-Fine sand was selected as the porous media for the release experiments based on its white coloring which enabled clear observation of the dyes used to visualize the spills. The properties of the Federal-Fine sand are given in Table 3-1.

Table 3-1. Properties of Ottawa Federal-Fine Sand.

Parameter	Federal-Fine Sand
Specific Gravity	2.65
D60/D10	1.67
Hydraulic Conductivity [cm/s]	0.0051
Capillary zone height [cm]	24 ± 1

Source: Mamonkina, 2011

For the smaller weeklong-duration ethanol and methanol blend experiments, the sand was packed in the cells using a semi-dry packing method (Stafford et al. 2009) used in previous work. In this semi-dry packing procedure, the sand was deposited in 2 cm

lifts. For each lift, sand was poured into the cell using a small beaker positioned at the top lip of the wall of the cell. To limit heap formation during this process, the beaker was continuously moved across the width of cell as the sand was poured from the beaker. Throughout the deposition of the sand, a water level in the side wells of the apparatus was maintained such that the deposited sand was completely saturated, but was not submerged. When a lift height of 2 cm was reached, the sand was then tamped down and compacted with an acrylic bar as a pestle.

Unlike the shorter-term ethanol and methanol blend releases, the larger (50 x 55 x 1.5 cm) cell was packed using a saturated packing method for the 75-mL M15 release. In this packing method, a layer of water was maintained above the level of the sand while packing. As with the unsaturated packing, the sand was loaded into the cell in 2 cm lifts and tamped down.

During packing, 19-gauge stainless steel needles (Sigma Aldrich Model Z219363 and Z219371) were embedded in the media as spill injection and pore-water sampling ports. These needles were installed in the cell once the height of the packed sand reached the intended vertical location of the port. The remaining media was then packed around the emplaced needles.

For the 75-mL M15 release, six sampling ports were installed in addition to the injection port to collect pore-water concentration measurements (Figure 3-2). The locations of these ports were chosen based on the flow patterns observed in the tracer test to most effectively capture the movement of the pore water. Ports 1 and 2 were placed directly downstream of the source, with ports 3 and 4 in the unsaturated zone downstream

of the source below ports 1 and 2. Ports 5 and 6 were placed close to the outlet at the water table and in the saturated zone, respectively.

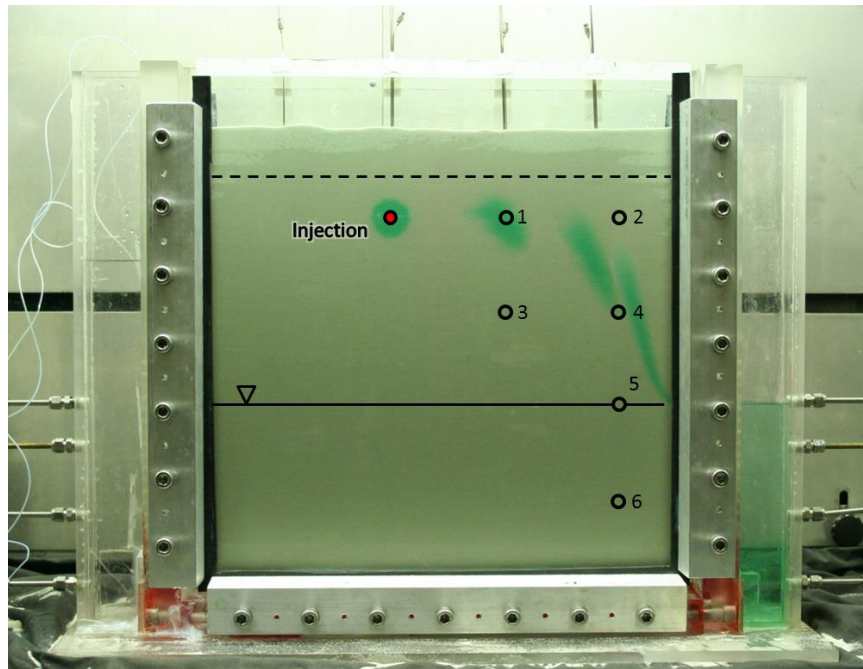


Figure 3-2. Diagram of injection and sampling ports and tracer study.

Once the cell was fully packed, any air bubbles remaining in the well screens were removed by initiating forward and reverse water flows through the cell. When a release experiment was completed, the cell was emptied and rinsed clean before repacking for the next release to prevent contamination.

Deionized water was delivered to the system at a constant rate via a Masterflex pump (Cole-Parmer Model #7521-50). The height of the water table was set by ports at the outlet of the cell. The water table height then determined the vertical position of the injection point, located four centimeters below the top of the capillary fringe (Figure 3-2) based on visual observation of water saturation. A distinct wet/non-wet transition was observed, occurring where water saturation dropped significantly with height.

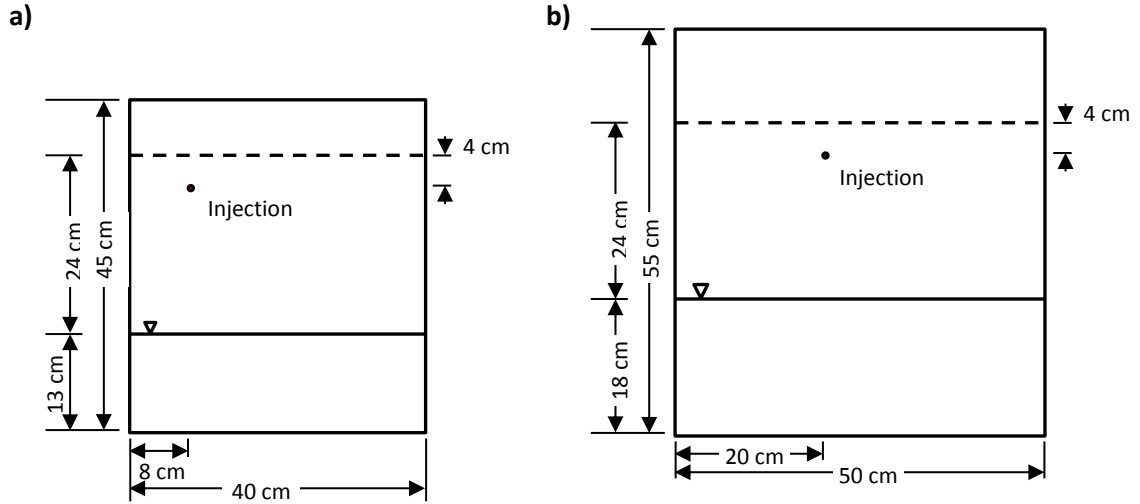


Figure 3-3. Layout of bench-scale cells used in (a) ethanol-blended fuel experiments and (b) methanol-blended fuel experiments.

3.1.2 Cell Hydraulics

Flow in the cell was based on the parameters of an analogue pilot-scale model aquifer. The flow rate in the 8 m³ pilot scale tank was 90 gal/day, corresponding to flow rates of 0.285 and 0.591 mL/min in the smaller and larger cells, respectively.

The flow rate of the larger bench-scale 2D cell was calculated by scaling the flow of the pilot-scale tank using

$$Q_{bs} = \left(\frac{A_{bs}}{A_{ps}} \right) \times Q_{ps} = \left(\frac{1.5\text{cm} \times 18\text{cm}}{180\text{cm} \times 60\text{cm}} \right) \times 90 \text{ gal/day} = 0.591 \text{ mL/min}, \quad (3-1)$$

where

A_{bs} = cross-sectional area of the bench-scale cell saturated zone [cm²]

A_{ps} = cross-sectional area of the pilot-scale tank saturated zone [cm²]

Q_{bs} = water flow rate of bench-scale cell saturated zone [gal/day]

Q_{ps} = water flow rate of pilot-scale tank saturated zone [gal/day].

A similar calculation was performed for the smaller 2D cell where

$$A_{bs} = 1\text{cm} \times 13\text{cm} , \quad (3-2)$$

giving a flow rate of 0.285 mL/min.

The Darcy velocity in the larger cell is calculated as

$$v = \frac{Q_{bs}}{A_{bs}} = \frac{0.591\text{mL}/\text{min}}{27\text{cm}^2} = 0.22\text{ cm}/\text{min} = 31.5\text{ cm}/\text{day} . \quad (3-3)$$

Similarly for the smaller cell,

$$v = \frac{Q_{bs}}{A_{bs}} = \frac{0.285\text{mL}/\text{min}}{13\text{cm}^2} = 0.22\text{ cm}/\text{min} = 31.5\text{ cm}/\text{day} . \quad (3-4)$$

Table 3-2. 2D Cell Characteristics

	Smaller Cell (40 cm x 45 cm x 1 cm)	Larger Cell (50 cm x 55 cm x 1.5 cm)
Darcy velocity [cm/day]	31.5	31.5
Flow rate [mL/min]	0.285	0.591
Spill volume/area ratio [cm ³ /cm ²]	0.5	
Close-packed media porosity	0.351 ⁽¹⁾	0.41
Water table height [cm]	13	18

⁽¹⁾Mamonkina, 2011

3.1.3 Blended Fuels

Each blended fuel comprised a volume percent of alcohol and an LNAPL mixture. Two-hundred proof ethyl alcohol and methanol were used as the alcohols in the blended fuels. The LNAPL mixture consisted of hydrocarbon components commonly found in gasoline: benzene, toluene, *m*-xylene, 1,2,4-trimethylbenzene (TMB), and *iso*-octane.

Table 3-3. Physical-chemical properties of alcohols and LNAPL hydrocarbon components.

	MW	ρ [g/cm ³]	Viscosity [cp]	Aq. Solubility [mg/L]	Surface Tension [dynes/cm]	Interfacial Tension (HC-Aq.) [dynes/cm]	Mass Fraction in LNAPL
Ethanol	46.1	0.789	1.1	Infinite	22	n/a	-
Methanol	32.0	0.792					-
Benzene	78.1	0.879	0.6	1780	28	35	0.021
Toluene	92.1	0.876	0.56	515	28	36	0.056
<i>m</i> -Xylene	106.2	0.864	0.58	162	29	36	0.117
1,2,4-TMB	120.2	0.878	0.77	57	29	-	0.294
<i>iso</i> -Octane	114.2	0.688	0.47	0.7	20	-	0.512
							1.000

The ethanol-blended fuels were injected in 20 mL spill volumes as in the initial ethanol blend experiments. This 20-mL volume was originally chosen to give a spill volume to aquifer area ratio of 0.5. For the smaller cell (40 cm x 45 cm x 1 cm) in which the ethanol blend experiments were conducted, this ratio is calculated as

$$\frac{V_{spill}}{A_{spill}} = \frac{20\text{mL}}{40\text{cm}^2} = 0.5 \text{ cm}^3/\text{cm}^2. \quad (3-5)$$

To facilitate the comparison of the ethanol- and methanol-blended fuels, an injection volume of 30 mL was selected for the methanol-blended fuel experiments conducted in the larger cell (50 cm x 55 cm x 1.5 cm). This 30-mL spill volume was scaled from the 20-mL ethanol blend releases in the smaller cell based on the thickness of the two cells. Scaling the spill volume in this way generated profile spill areas in the larger cell comparable to those from the 20-mL spills in the smaller cell.

3.1.4 Dyes and Tracers

To aid in the visualization of the releases, dyes were added separately to the NAPL and alcohol components of the blended fuels before mixing. Hydrophobic Sudan Red (Sigma-Aldrich: CAS# 6368-72-5) was added to the NAPL mixture at a concentration of 100 mg/L and hydrophilic Fluorescein (Sigma-Aldrich: CAS# 2321-07-05) was likewise added to the alcohols at a 100 mg/L concentration.

Prior to each blended-fuel release, an aqueous tracer of dilute propylene glycol was injected into the packed cell. With the same injection volume as the fuel releases, the tracers were used to determine seepage velocity and flow patterns through the cell. The movement of each tracer, colored green by the propylene glycol, was recorded in digital photographs taken regularly as the tracer migrated through the system (Figure 3-3).

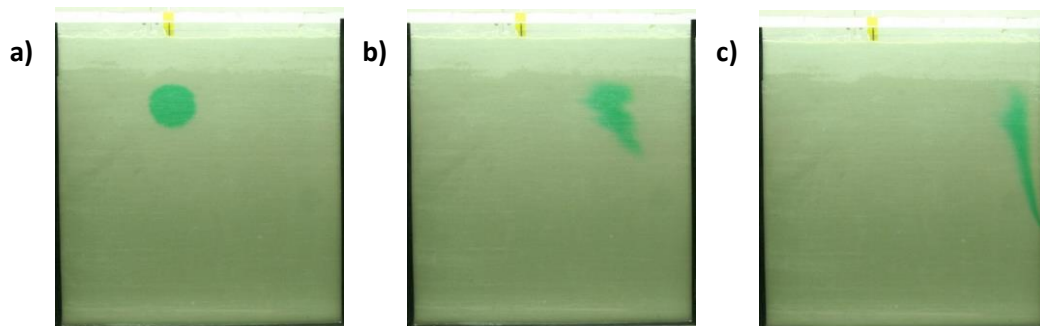


Figure 3-4. Visualization of propylene glycol tracer (a) immediately after injection, (b) 24 hours after injection and (c) 48 hours after injection.

3.1.5 Methods of Analysis

For the one-week duration of each experiment, digital still photographs were taken of each release. Image processing of these photographs was accomplished using the software program ImageJ (Wayne Rasband, U.S. National Institutes of Health, Bethesda, MD, USA). In ImageJ, the outline of the residual NAPL was first manually traced.

Reference dimensions within the image were set and the area of the traced residual was then computed via pixel count.

From the measured area of the NAPL residual, the saturation of the region was determined. The total pore volume contaminated by the NAPL, V_{cont} , was calculated as

$$V_{cont} = \varepsilon \times A_{spill} \times w , \quad (3-6)$$

where

ε = cell porosity

A_{spill} = area of NAPL residual source [cm^2]

w = depth of the cell.

Using the contaminated pore volume, the NAPL (oil) saturation, θ_{NAPL} , was calculated as

$$\theta_{NAPL} = \frac{V_{NAPL}}{V_{cont}} , \quad (3-7)$$

where

V_{NAPL} = volume of NAPL (hydrocarbons) in the fuel mixture [cm^3].

CHAPTER 4: RESULTS AND DISCUSSION

4.1 Methanol Blend Releases

The methanol-blended fuel releases (M15, M25, M50 and M85) were conducted in the larger (50 cm x 55 cm x 1.5 cm) 2D cell. Thirty milliliters of each methanol blend were injected into the capillary zone of the cell under similar conditions for all four releases.

4.1.1 M15 Release

A 30-mL release of the methanol blend M15 (15 % v/v methanol) was injected into the capillary zone. The visualization of this release is shown in Figure 4-1.

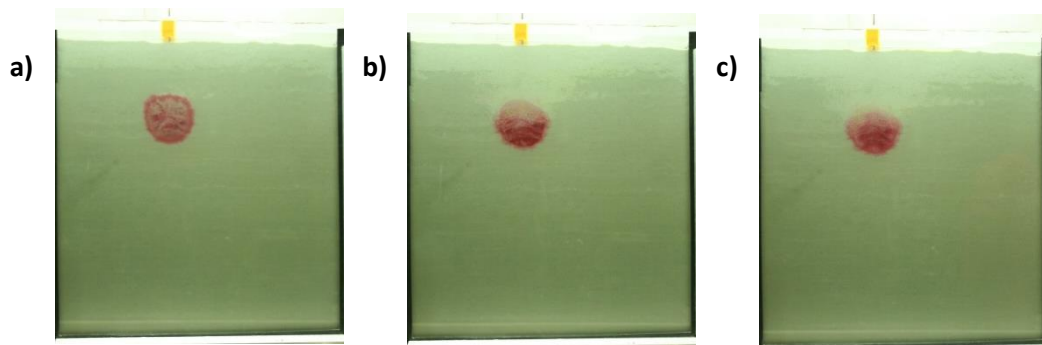


Figure 4-1. Visualization of M15 release in the capillary zone (a) after injection, (b) 24 hours after injection, and (c) one week after injection.

The high percentage of NAPL in this blend generated a high-saturation NAPL source upon injection with no phase separation visible due to the low methanol content of the blend. Twenty-four hours after injection, depression of the capillary fringe was observed. At this time, the NAPL in the source zone appeared to have been redistributed while the areal extent of the source remained relatively unchanged. After one week, little recovery in the height of the capillary fringe was observed from the visualization results.

4.1.2 M25 Release

A release of 30 mL M25 was injected into the capillary zone as shown in Figure 4-2. Shortly after the injection of M25, a small amount of methanol had phase separated and entered the pore water as evidenced by the yellow Fluorescein fringe at the upper edge of the NAPL source. After 24 hours, further phase separation of methanol had occurred accompanied by slight spreading of the NAPL source and capillary fringe depression. After one week, the capillary fringe had not yet recovered and noticeable amounts of NAPL were present downstream of the source.

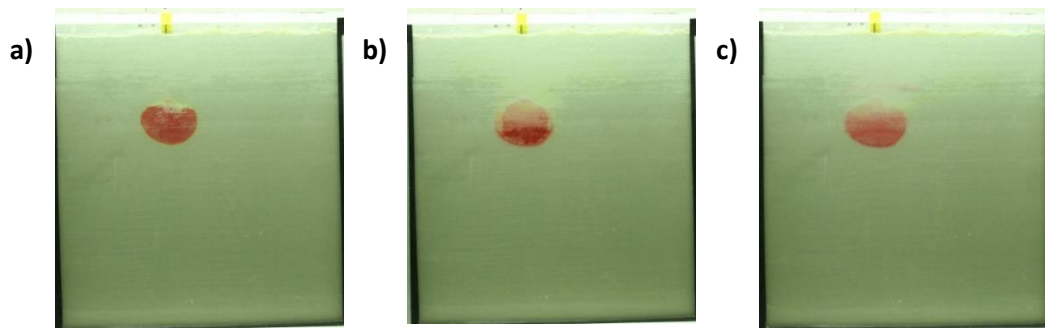


Figure 4-2. Visualization of M25 release in the capillary zone (a) after injection, (b) 24 hours after injection, and (c) one week after injection.

4.1.3 M50 Release

Thirty milliliters of the intermediate methanol blend M50 were released in the capillary zone as shown in Figure 4-3. Immediately after injection of the M50 blend, a faint yellow halo was observed surrounding the NAPL source, most prominent on the upper edge, indicating phase separation of the methanol.

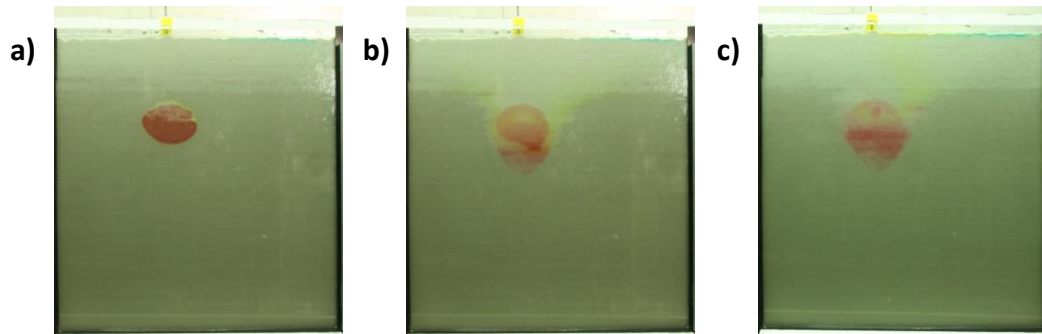


Figure 4-3. Visualization of M50 release in the capillary zone (a) after injection, (b) 24 hours after injection, and (c) one week after injection.

After 24 hours, the higher methanol content in the M50 blend resulted in greater depression of the capillary fringe relative to that observed for M15 and M25. Further, the fuel's NAPL content produced sufficient saturation in the residual NAPL source to temporarily restrict flow through the region, trapping a portion of the methanol upstream of the NAPL. The NAPL source zone had increased in area since the time of injection, expanding downwards, and, at this time (24 hours), a lower-saturation zone across the middle of the NAPL source was emerging as the methanol began to break through the high-saturation source zone.

One week after injection, the methanol had migrated downstream of the source and some recovery in the capillary fringe height was observed. The middle region of lower saturation from the methanol breakthrough was clearly visible in the NAPL source, though the total area of the source zone remained relatively unchanged after its initial expansion in the first 24 hours after injection. Trace amounts of NAPL were also observed downstream of the source.

4.1.4 M85 Release

A 30-mL injection of M85, a high-methanol content fuel blend, was conducted in the capillary zone as shown in Figure 4-4. The low NAPL content of the M85 fuel generated a low saturation residual source zone. Initial phase separation of the methanol was observed following the injection as a distinct yellow halo surrounding this source zone.

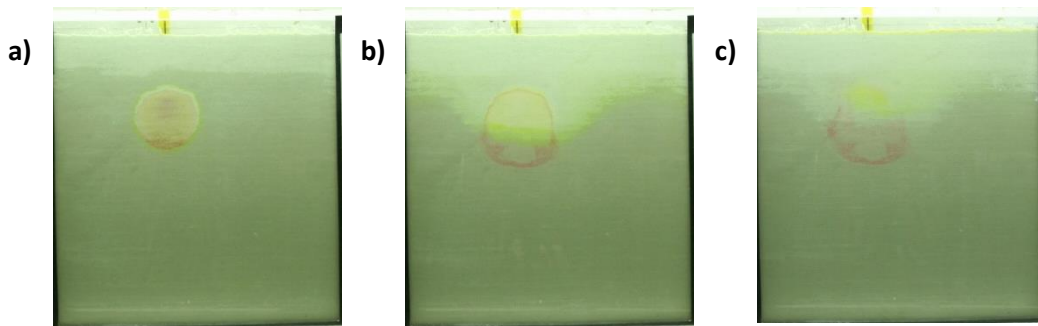


Figure 4-4. Visualization of M85 release in the capillary zone (a) after injection, (b) 24 hours after injection, and (c) one week after injection.

Twenty-four hours later, the injected NAPL was concentrated at the edge of the residual source, forming a thin higher-saturation ring surrounding the low saturation center. As with the M50 injection, the NAPL source zone had spread downwards, enlarging the area of the spill. The decrease in surface tension from the large amount of methanol in the fuel caused a substantial depression in the capillary fringe. A minimal amount of methanol remained upstream of the source at this time due to the small reduction in flow through the NAPL source from the low residual saturation. Recovery of the capillary fringe one week after injection was greater than that observed for the lower methanol content fuels. The NAPL source zone remained relatively unchanged.

4.1.5 Summary of Methanol Blend Releases

Trends in spill behavior were observed in the visualization of the methanol-blended fuel releases. In all cases, capillary fringe depression occurred within 24 hours of injection, with some recovery for the higher methanol content fuels after one week.

Spreading of the NAPL residual source zone was observed in all blends. As described previously, this spreading was quantified via image processing. Initial saturation and final values for saturation and contaminated pore volume were calculated 10 minutes and one week after injection, respectively (Table 4-1 and Figure 4-5).

Saturation decreased over the duration of each experiment with the spreading of the source zone. Across the blends, spreading of the source increased with increasing methanol content. Correspondingly, final contaminated pore volume increased, while final saturations decreased with increasing methanol content. M50, however, was unique in the formation of a lower NAPL saturation middle zone following release.

Table 4-1. NAPL saturations and pore volume impacted by NAPL for 30-mL methanol fuel blend releases.

	M15	M25	M50	M85
Initial Saturation	0.703	0.626	0.388	0.085
Final Saturation	0.621	0.509	0.244	0.047
Final Contaminated Pore Vol. (cm ³)	41.1	44.2	61.5	95.3

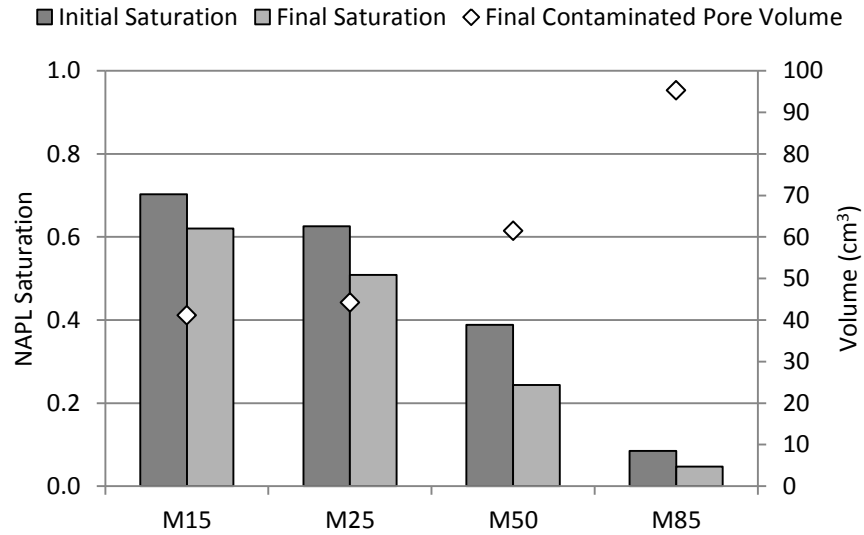


Figure 4-5. NAPL saturation and pore volume impacted by NAPL for 30-mL methanol fuel blend releases.

4.2 Duplicate Ethanol Blend Releases

Previous experimental releases (Mamonkina 2011) of ethanol-blended fuels were duplicated. In these visualization experiments, 20 mL of E15, E25, E50 and E85 blended fuels were injected in the capillary zone of the smaller (40 cm x 45 cm x 1 cm) 2D cell, similar to the methanol-blended fuel releases. The conditions of these duplicate releases were similar across all tested ethanol blends and matched those of the original release experiments.

4.2.1 Results

The outcomes of the four duplicate experiments corroborated the results obtained previously. General stages of fuel behavior identified in the initial study (Mamonkina 2011) were again observed in these releases: the injection of fuel into the capillary zone,

the partitioning of ethanol into the aqueous phase and the redistribution of the NAPL phase. The visualization of the duplicate releases is shown in Figure 4-6.

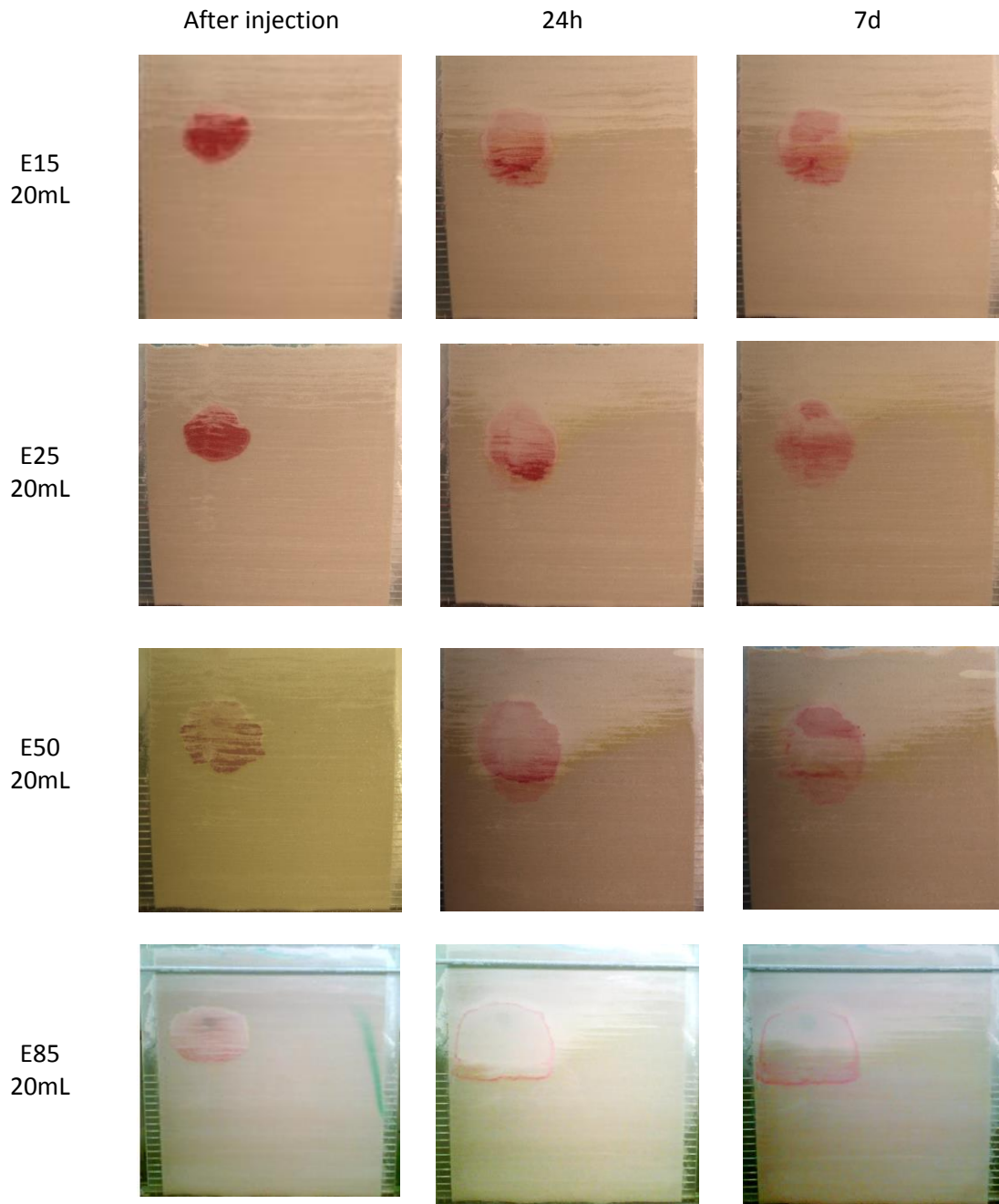
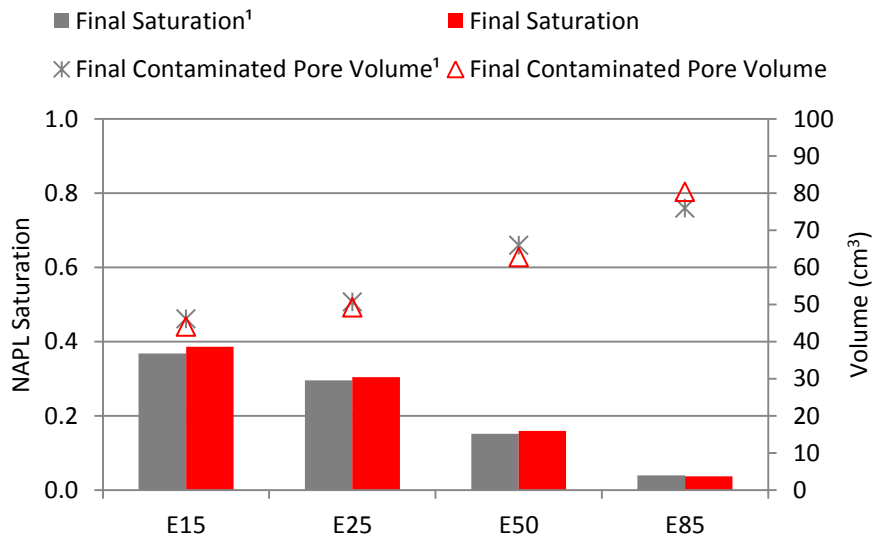


Figure 4-6. Duplicate visualization experiments of ethanol-blended fuel releases

As before, higher residual NAPL saturations from the lower ethanol content fuels suggested water flow bypassing which leads to mass transfer-limited dissolution of BTEX from NAPL and thus the potential for persistent long-lived low BTEX concentrations in the downstream pore water. Furthermore, for the higher ethanol content fuels, low residual NAPL saturations indicated good flow of pore water through the residual source that may result in initially greater, but shorter-lived BTEX pore water concentrations.

Numerical analysis of the duplicate releases yielded values similar to those obtained in the initial experiments. A comparison of the numerical results between the initial and duplicate experiments is given in Figure 4-7.



¹Mamonkina, 2011

Figure 4-7. NAPL saturations and contaminated pore volumes for initial and duplicate ethanol-blended fuel releases

Table 4-2. NAPL saturations and contaminated pore volumes for initial and duplicate ethanol-blended fuel releases.

	E15	E25	E50	E85
Final Saturation				
Run 1 ¹	0.368	0.296	0.152	0.039
Run 2	0.386	0.305	0.159	0.037
Final Contaminated Pore Volume [cm ³]				
Run 1 ¹	46.1	50.7	65.9	76.0
Run 2	44.0	49.2	62.7	80.3

¹Mamonkina, 2011

4.3 Comparison of Methanol and Ethanol Releases

The methanol and ethanol blend releases follow the general stages of formation of a residual NAPL source, phase separation, depression of the capillary fringe and NAPL redistribution. Visualizations of corresponding ethanol and methanol blends are compared in Figures 4-8, 4-9, 4-10 and 4-11.

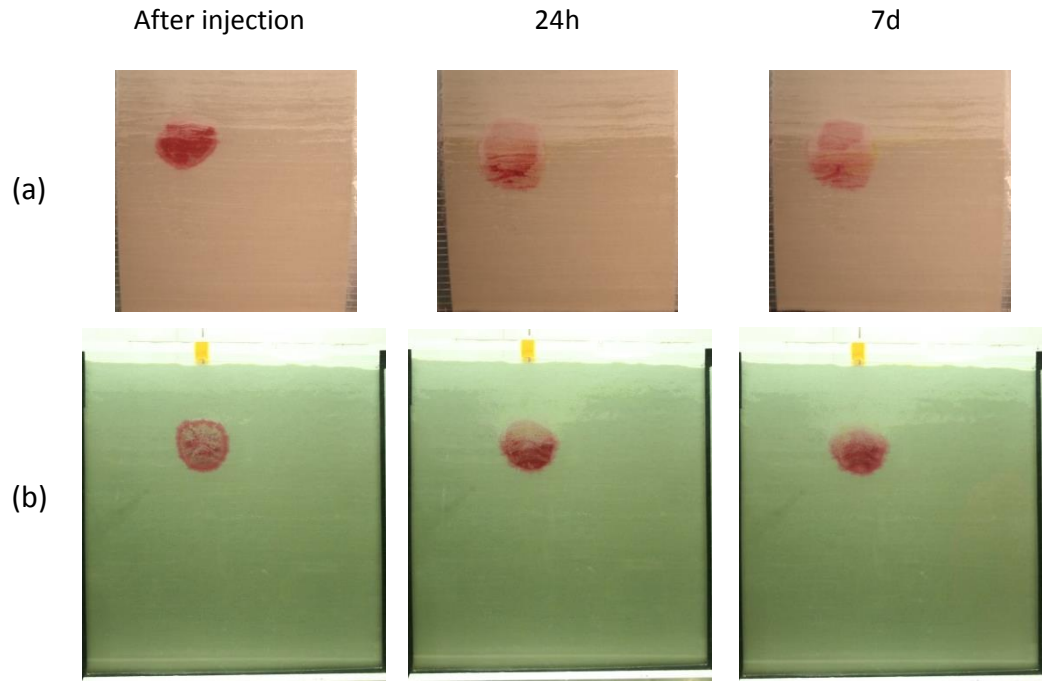


Figure 4-8. Visual comparison of (a) 20-mL E15 and (b) 30-mL M15 releases.

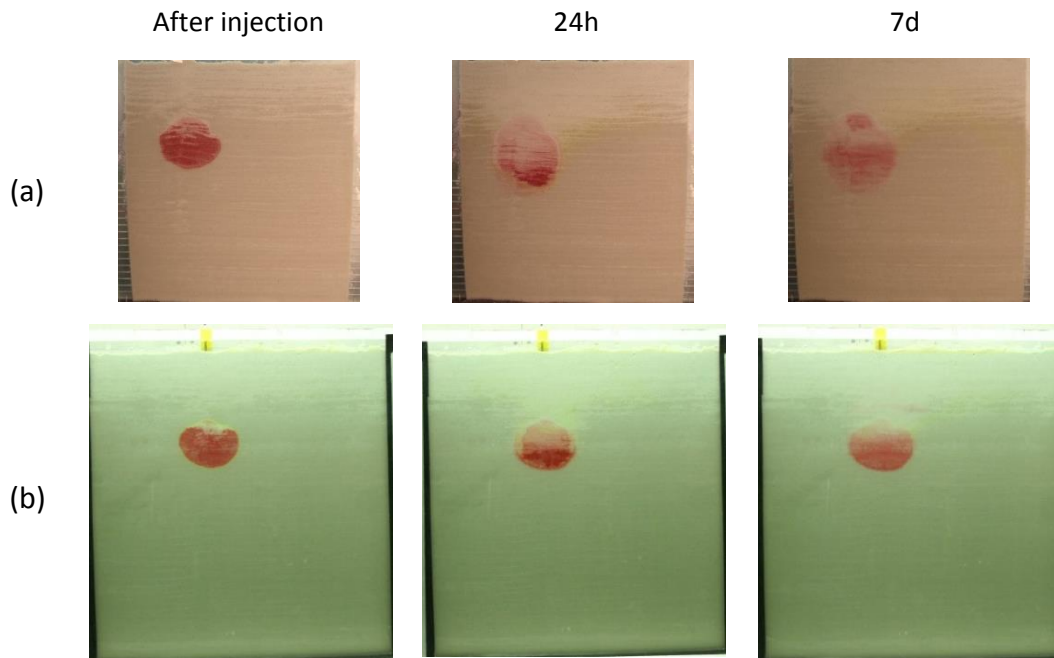


Figure 4-9. Visual comparison of (a) 20-mL E25 and (b) 30-mL M25 releases.

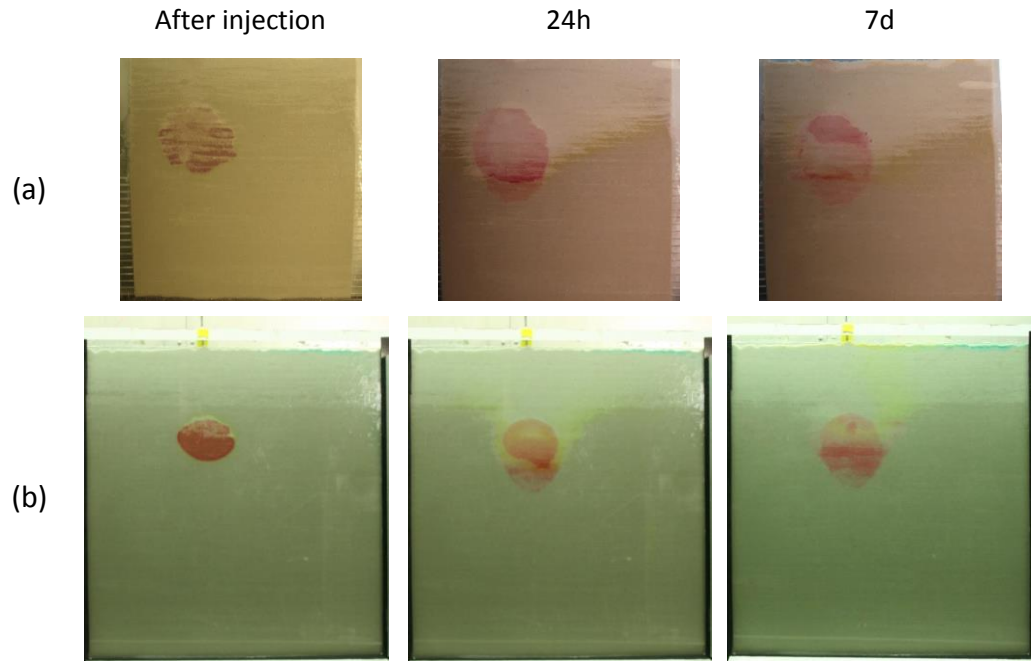


Figure 4-10. Visual comparison of (a) 20-mL E50 and (b) 30-mL M50 releases.

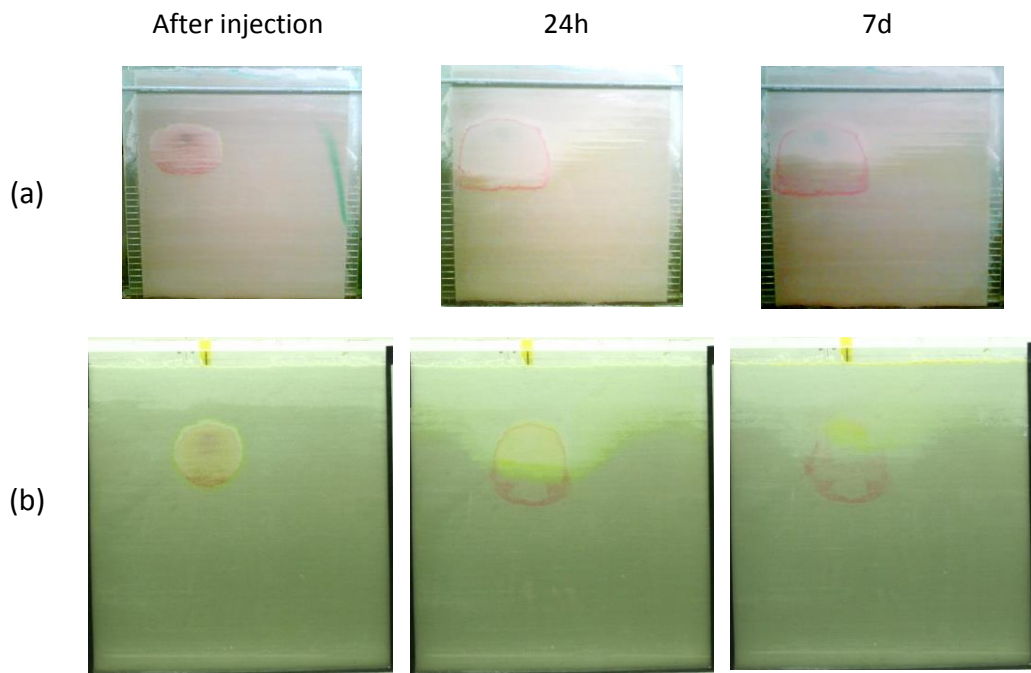


Figure 4-11. Visual comparison of (a) 20-mL E85 and (b) 30-mL M85 releases.

Overall, for both methanol and ethanol, capillary fringe depression and spreading of the NAPL source increased with increasing alcohol content in the fuels. Additionally, in the low alcohol content fuels (up to 25 vol. % alcohol), little phase separation was observed in both the ethanol and methanol blends likely due to the small amount of alcohol in the fuels.

The alcohols were differentiated in several aspects. The behavior of methanol and ethanol fuels diverged on the NAPL redistribution of the intermediate alcohol content fuels (25 and 50 vol. % alcohol). For E25 and E50, ethanol was trapped upstream of the highly saturated residual NAPL source zone, eventually breaking through and forming a horizontal middle zone of lower saturation and higher flow in the residual NAPL one week after release. The trapping of alcohol upstream and subsequent breakthrough occurred much sooner for M50, with a distinct middle low saturation zone emerging just 24 hours after injection and appearing greatly reduced after one week. A middle lower saturation zone was never formed in the M25 case, with NAPL redistribution more similar to the low methanol content M15 blend than M50. Though capillary fringe depression was observed in all methanol and ethanol blend releases, the capillary depression for the methanol blends was less than that of their ethanol blend counterparts.

A quantitative comparison of the ethanol and methanol-blended fuels is given in Figure 4-12. Overall, the saturation of the NAPL source zone one week after injection (the final saturation) was greater for the methanol-blended fuels than for their ethanol counterparts. However, the normalized spill area was larger for the ethanol blends than for their corresponding methanol blends.

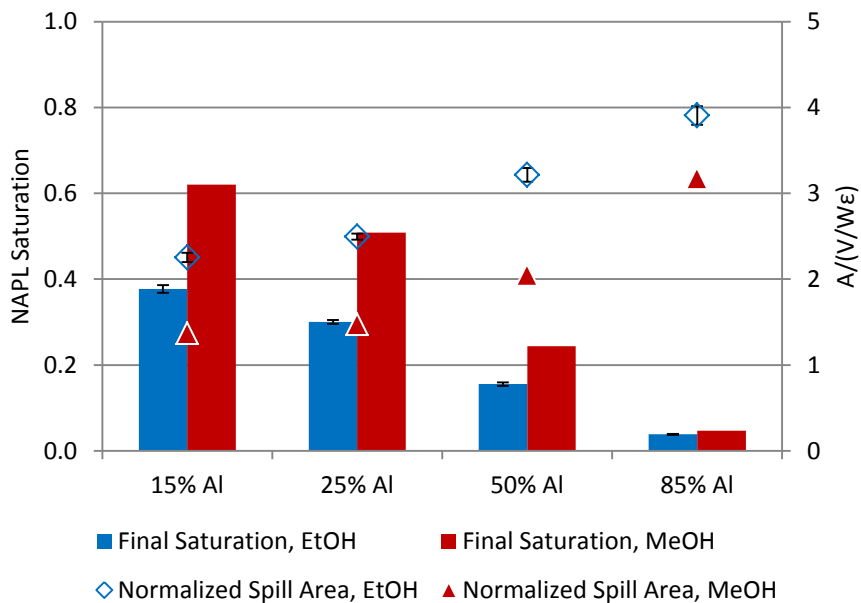


Figure 4-12. Final saturations and normalized spill areas for alcohol blended fuels.

Table 4-3. Final saturations and normalized spill areas for alcohol blended fuels.

	15% AI	25% AI	50% AI	85% AI
Final Saturation, EtOH	0.377	0.301	0.156	0.038
Final Saturation, MeOH	0.621	0.509	0.244	0.047
A/(V/Wε), EtOH	2.254	2.496	3.216	3.907
A/(V/Wε), MeOH	1.37	1.474	2.049	3.175

4.4 75-mL M15 Release and Porewater Measurements

4.4.1 Visualization Study

Visualization data of the 75-mL release are given in Figure 4-13.

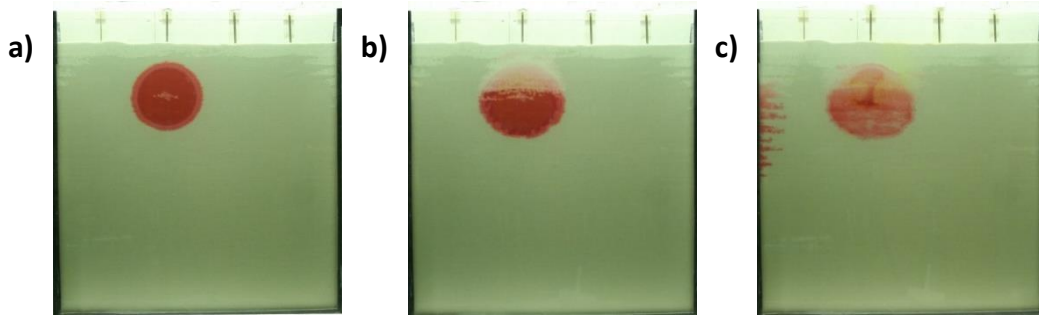


Figure 4-13. Visualization of 75-mL M15 release in the capillary zone (a) after injection, (b) 24 hours after injection, and (c) one week after injection.

As with the smaller 30-mL spill, a high-saturation NAPL source zone was generated by the 75-mL M15 release with no visible phase separation. After 24 hours, the NAPL had redistributed, accompanied by a slight decrease in the capillary fringe. Additionally, in this time, the area of the source zone had enlarged dissimilar to the smaller M15 spill, in which the source area remained unchanged. One week after injection, the capillary fringe height had decreased and phase separation was evident with fluorescein dye visible above the source.

4.4.2 Pore-water Concentration Measurements

Following the fuel injection, one-milliliter pore-water samples were drawn from the six sampling ports at regular intervals. The samples then were analyzed using a gas chromatograph (Hewlett Packard Model #5890) with a Supelco capillary column (Model SPB-5, 30 m x 0.53 mm x 5 μ m) and an OI Analytical flame ionization detector (FID) to measure pore-water concentrations of methanol, the BTX compounds benzene, toluene,

and m-xylene and TMB (1,2,4-trimethylbenzene). These methanol, BTX and TMB concentration measurements are given in Figures 4-14, 4-15 and 4-16 for ports 1, 2 and 4, respectively.

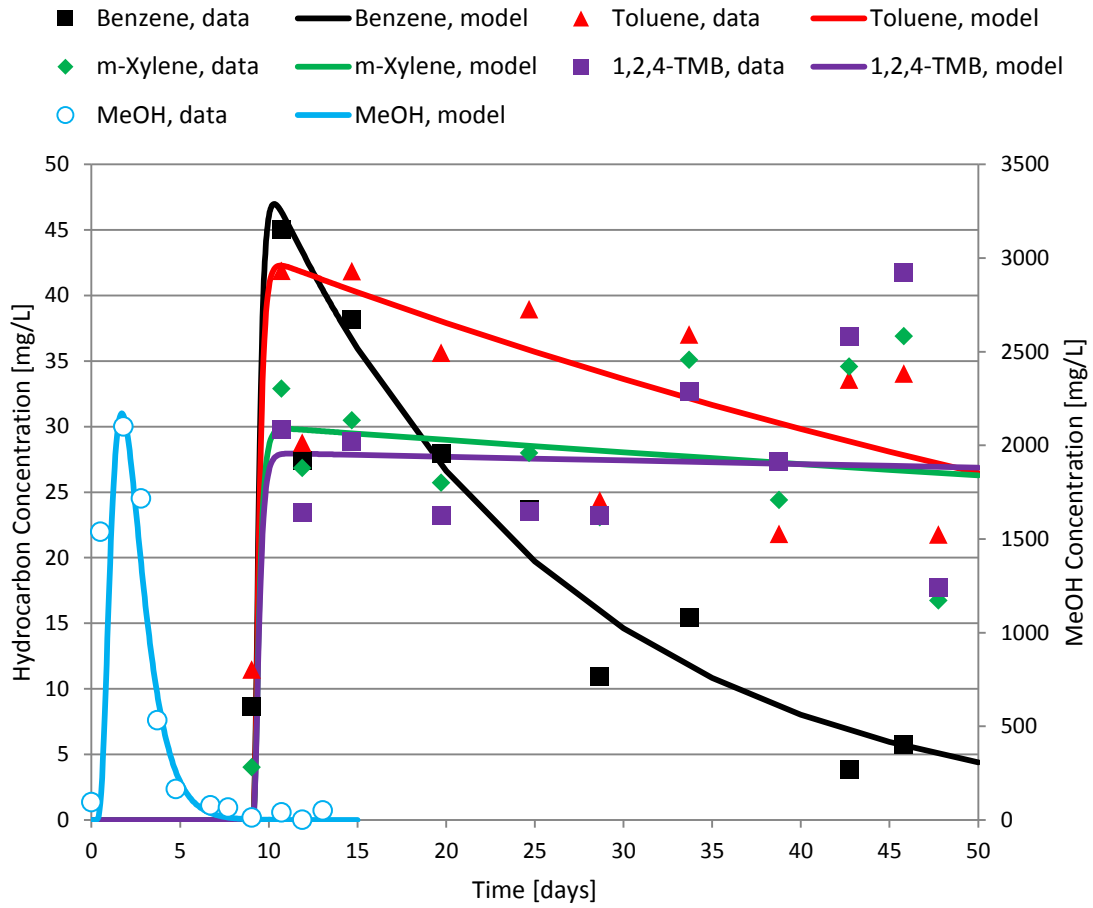


Figure 4-14. Port 1 measured hydrocarbon and methanol concentrations and model (Equations 4-6 and 4-1) values.

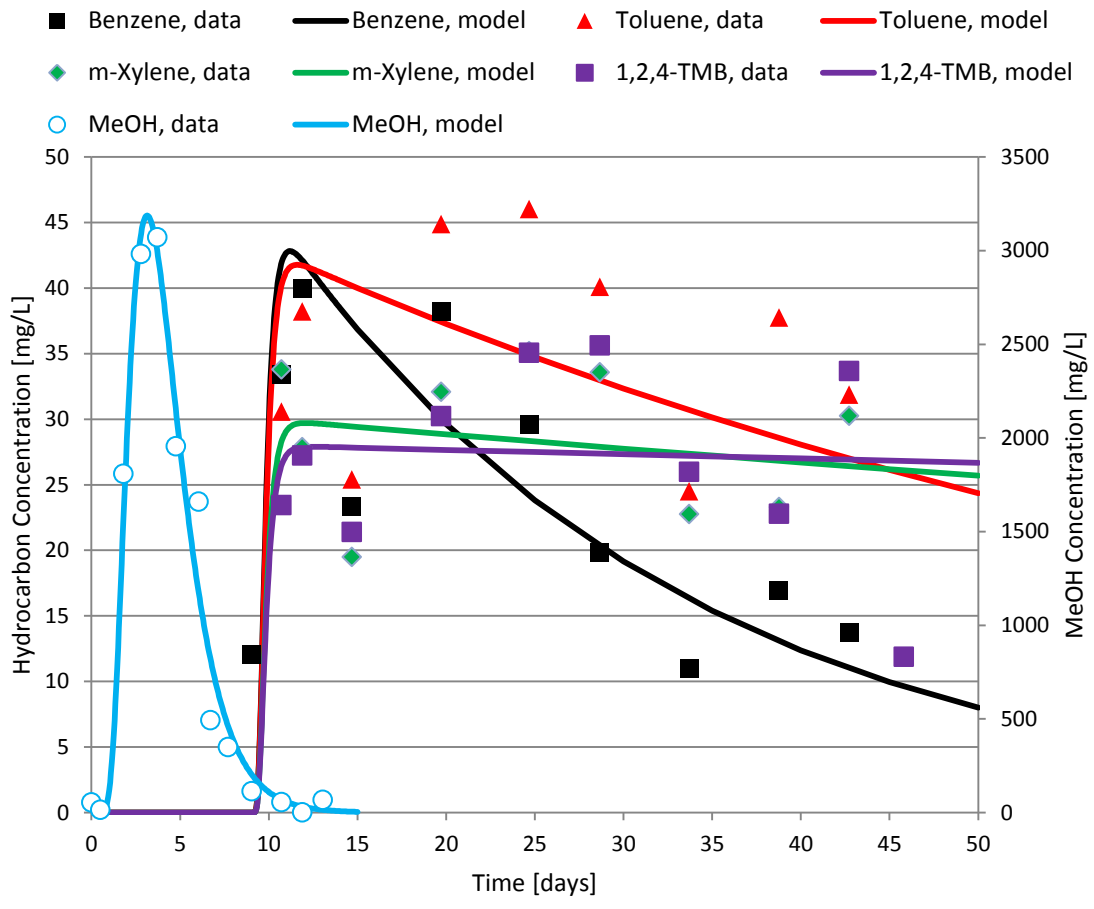


Figure 4-15. Port 2 measured hydrocarbon and methanol concentrations and model (Equations 4-6 and 4-1) values.

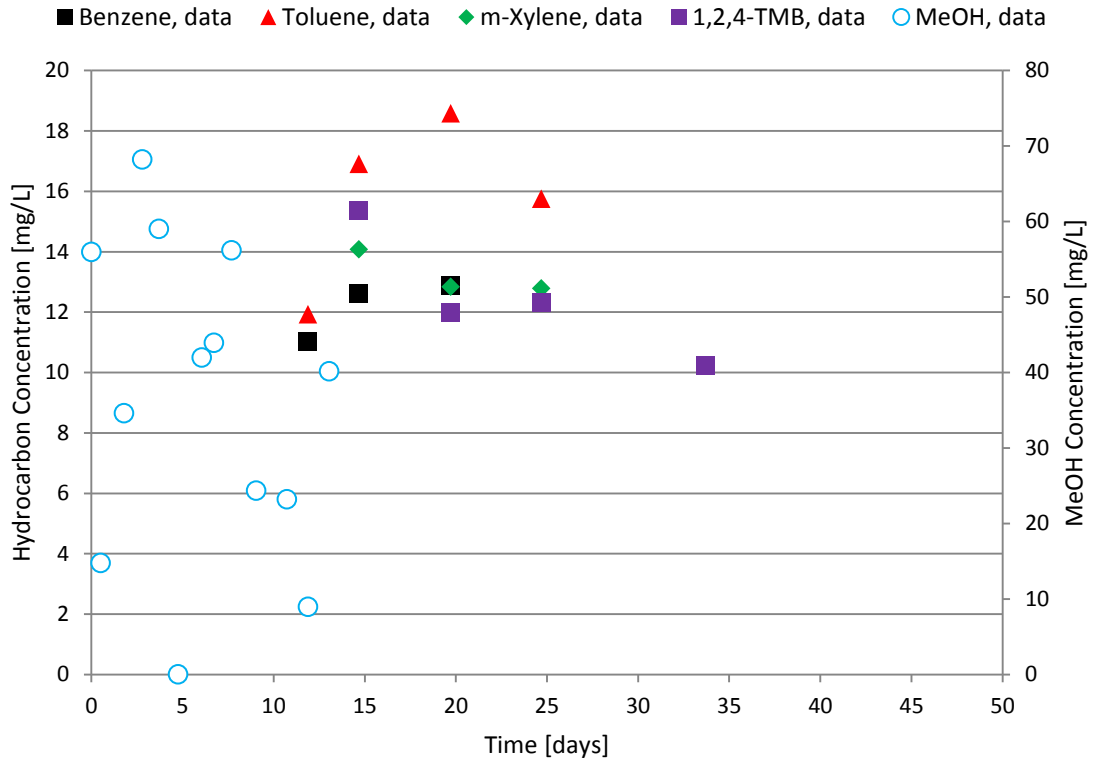


Figure 4-16. Port 4 measured hydrocarbon and methanol concentrations

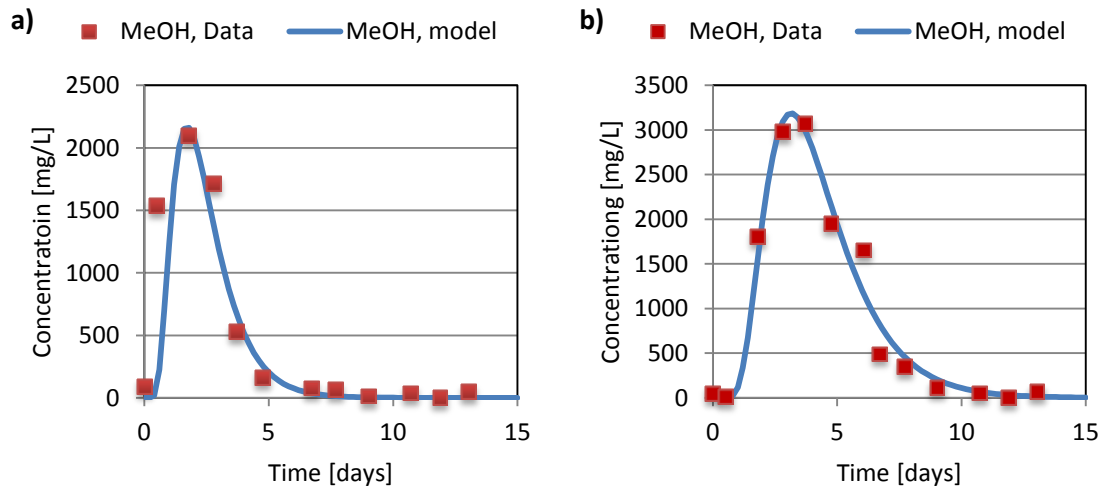


Figure 4-17. Methanol measured concentrations and model curves (Equation 4-1) at (a) Port 1 and (b) Port 2.

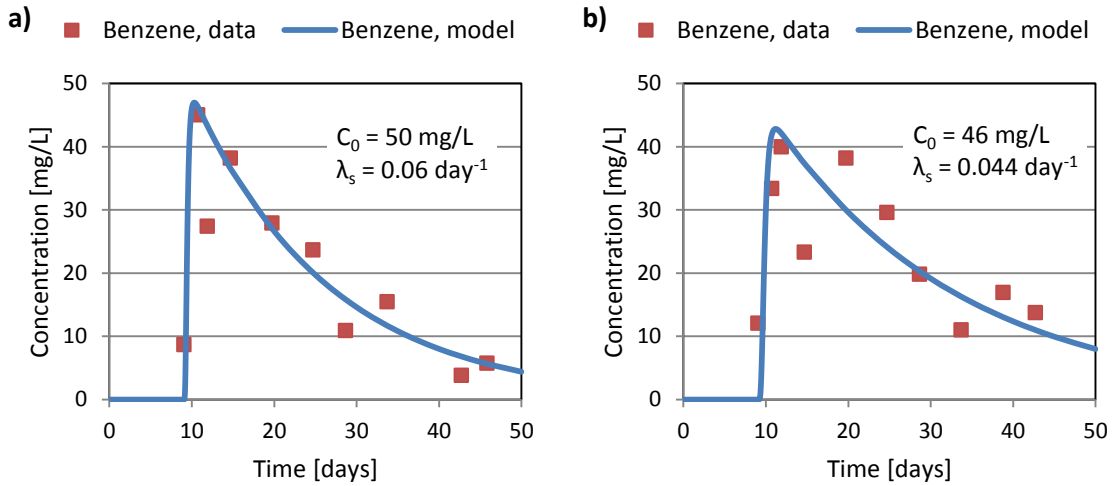


Figure 4-18. Benzene measured concentrations and model curves (Equation 4-6) at (a) Port 1 and (b) Port 2.

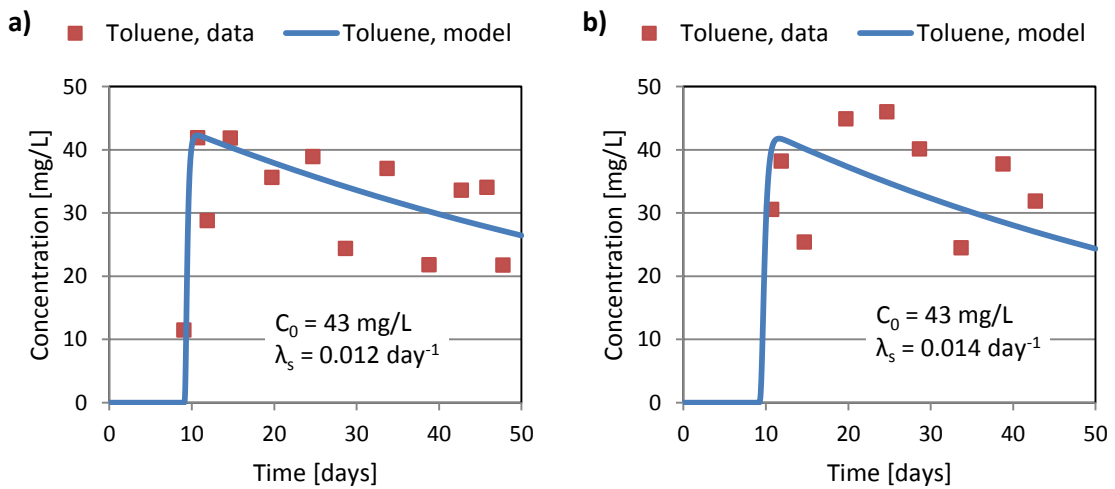


Figure 4-19. Toluene measured concentrations and model curves (Equation 4-6) at (a) Port 1 and (b) Port 2.

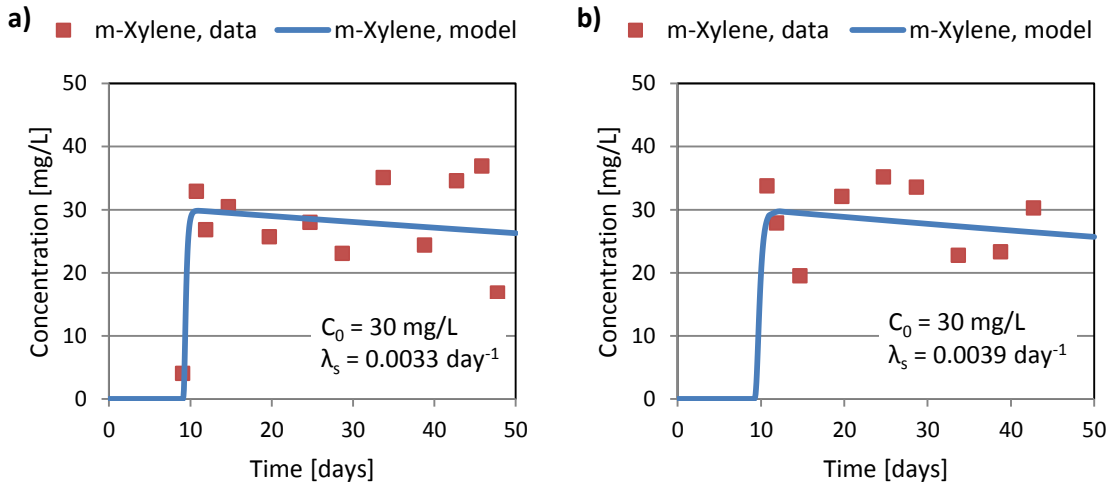


Figure 4-20. m-Xylene measured concentrations and model curves (Equation 4-6) at (a) Port 1 and (b) Port 2.

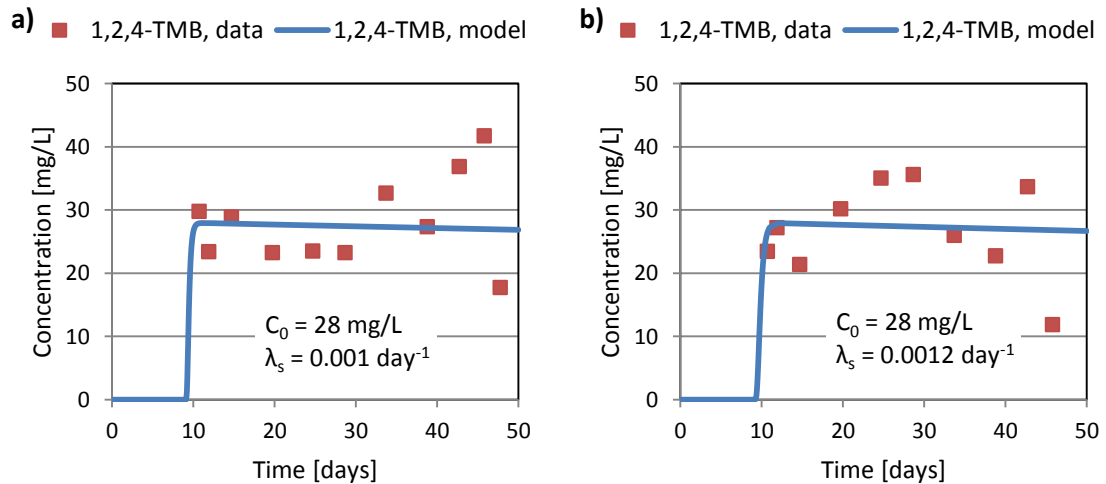


Figure 4-21. 1,2,4-TMB measured concentrations and model curves (Equation 4-6) at (a) Port 1 and (b) Port 2.

Ports 1 and 2 directly downstream of the injection point showed similar trends in BTX and TMB concentrations. BTX and TMB compounds were first detected in these two ports approximately 11 days after the fuel release, with subsequent toluene, m-xylene and TMB concentrations remaining relatively constant for the remainder of the

experiment at around 30 mg/L. Benzene concentrations rapidly increased from low initial measurements to maximums of 45.0 and 40.0 mg/L in ports 1 and 2, respectively, followed by a steady decrease in concentration.

At port 4, below and downstream of the source, low concentrations of the BTX and TMB compounds (< 20 mg/L) were measured beginning twelve days after the fuel release. However, after 34 days, unlike at ports 1 and 2, BTX and TMB compounds were no longer detectable in the pore water. BTX and TMB compounds were not detected at ports 3, 5 and 6.

Six hours after the fuel release, methanol was detected in the first samples drawn from ports 1, 2 and 4. Maximum methanol concentrations in ports 1 and 2 were observed within days of the release with concentrations of 2100 mg/L two days after release and 3071 mg/L four days after release in port 1 and port 2, respectively. Subsequently, concentrations of methanol quickly declined and were no longer detectable in these two ports 14 days after the release. Over the same time frame, low methanol concentrations (< 80 mg/L) were registered in port 4, decreasing to undetectable levels after 14 days.

4.4.3 Pore-water Concentration Modeling

4.4.3.1 Plume Transport Model

Methanol:

The methanol concentrations measured downstream of the source were fitted using a one-dimensional slug injection into a flow field (Fetter 1993) given as

$$C_R(t_R, Pe) = \frac{E}{(t_R)^{1/2}} \exp\left(-\frac{Pe}{4t_R}(1 - t_R)^2\right), \quad (4-1)$$

for

$$E = (t_{Rmax})^{1/2} \cdot \exp\left(\frac{Pe}{4t_{Rmax}}(1 - t_{Rmax})^2\right), \quad (4-2)$$

$$t_{Rmax} = (1 + Pe^{-2})^{1/2} - Pe^{-1}, \text{ and} \quad (4-3)$$

$$C_R = C/C_{max}, \quad (4-4)$$

where

t_R = dimensionless time

t_{Rmax} = dimensionless time at which peak concentration occurs

C_{max} = peak concentration.

Hydrocarbons:

A 1-dimensional plume transport model incorporating a depleting source zone was used to characterize the concentrations measured downstream of the residual NAPL source. The model scenario is shown in Figure 4-22.

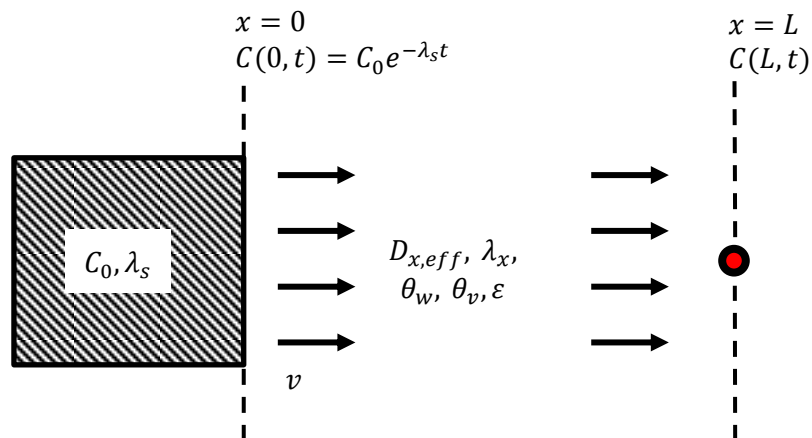


Figure 4-22. Plume transport model scenario.

A PDE based on a solute mass balance given as

$$\frac{\partial C}{\partial t} = D \frac{\partial^2 C}{\partial x^2} - v \frac{\partial C}{\partial x} - kC \quad (4-5)$$

was solved with the following initial and boundary conditions:

$$\text{I. C. : } C(x, 0) = 0$$

$$\text{B. C. 1: } C(0, t) = C_0 e^{-\lambda_s t}$$

$$\text{B. C. 2: } \frac{\partial C(\infty, t)}{\partial x} = 0 ,$$

where

C = concentration [mg/L]

t = time [days]

x = distance from the source [cm]

D = dispersion coefficient [cm²/s]

v = interstitial velocity [cm/day]

k = reaction rate constant [day⁻¹]

λ_s = first order source depletion rate constant [day⁻¹].

The solution to Equation 4-5 is

$$C(x, t) = \frac{C_0}{2} \exp\left(\frac{vx}{2D}\right) \exp(-\lambda_s t) \left[\begin{array}{l} \exp\left(y \sqrt{\frac{k + \frac{v^2}{4D} - \lambda_s}{D}}\right) \operatorname{erfc}\left(\sqrt{\left(k + \frac{v^2}{4D} - \lambda_s\right)t + \frac{x}{2\sqrt{Dt}}}\right) \\ + \exp\left(-y \sqrt{\frac{k + \frac{v^2}{4D} - \lambda_s}{D}}\right) \operatorname{erfc}\left(-\sqrt{\left(k + \frac{v^2}{4D} - \lambda_s\right)t + \frac{x}{2\sqrt{Dt}}}\right) \end{array} \right]. \quad (4-6)$$

This solution was then non-dimensionalized via the following quantities:

$$\begin{aligned} t^* &= \frac{tv}{L} & Pe &= \frac{vL}{D} \\ x^* &= \frac{x}{L} & Da &= \frac{kL}{v} \\ C^* &= \frac{C}{C_0} & Da_s &= \frac{\lambda_s L}{v}, \end{aligned}$$

where

L = distance from the source to sampling port [cm]

C_0 = initial concentration [mg/L]

t^* = dimensionless time

x^* = dimensionless distance

C^* = dimensionless concentration

Pe = Peclet number

Da = Damkohler number

Da_s = Damkohler number (source).

When non-dimensionalized, Equation 4-6 becomes

$$\begin{aligned} C^*(x^*, t^*) = & \\ \frac{1}{2} \exp\left(\frac{Pe \cdot x^*}{2} - Da_s t^*\right) & \left\{ \exp\left(x^* \sqrt{Pe \left(Da + \frac{Pe}{4} - Da_s\right)}\right) \operatorname{erfc}\left(\sqrt{t^* \left(Da + \frac{Pe}{4} - Da_s\right)} + \right. \right. \\ \left. \frac{x^*}{2} \sqrt{\frac{Pe}{t^*}}\right) & + \exp\left(-x^* \sqrt{Pe \left(Da + \frac{Pe}{4} - Da_s\right)}\right) \operatorname{erfc}\left(-\sqrt{t^* \left(Da + \frac{Pe}{4} - Da_s\right)} + \frac{x^*}{2} \sqrt{\frac{Pe}{t^*}}\right) \right\}. \end{aligned} \quad (4-7)$$

4.4.3.2 Theoretical Source Parameter Calculations

Theoretical source depletion rate constants λ_s and equilibrium aqueous concentrations C_{i0}^W were calculated based on the physical properties of the hydrocarbon components and the hydraulic characteristics of the experimental apparatus (Table 4-2).

In determining theoretical equilibrium concentrations, partition coefficients for each component were first calculated as (Garg and Rixey 1999)

$$K_i^{o-w} = \frac{1}{\gamma_i^o} \frac{\rho^o}{\rho^w} \frac{MW_{avg}^w}{MW_{avg}^o} \frac{1}{S_i}, \quad (4-8)$$

where

K_i^{o-w} = oil-water partitioning coefficient [$\text{cm}^3\text{-o}/\text{cm}^3\text{-w}$]

γ_i^o = activity coefficient of component i in the oil phase

ρ^o = oil phase density [g/cm^3]

ρ^w = density of water [g/cm^3]

MW_{avg}^w = average molecular weight of water [g/mol]

MW_{avg}^o = average molecular weight of the oil phase [g/mol]

S_i = solubility of pure component i in the oil phase.

From these partition coefficients, theoretical equilibrium aqueous concentrations for each hydrocarbon component were determined as

$$C_{i0}^w = \frac{C_{i0}^o}{K_i^{o-w}}, \quad (4-9)$$

where

C_{i0}^w = initial concentration of component i in the water phase [mg/L]

C_{i0}^o = initial concentration of component i in the oil phase [mg/L].

The volumetric flow rate of water was calculated as

$$Q = vA\varepsilon S_w, \quad (4-10)$$

where

Q = volumetric flow rate of water [cm^3/day]

v = seepage velocity [cm/day]

A = cross-sectional spill area

ε = porosity

S_w = water saturation.

The mass of oil in the source was calculated as

$$m_o = \rho_o S_o \varepsilon A L_s , \quad (4-11)$$

where

m_o = oil mass in the source zone

ρ_o = oil density

S_o = oil saturation

L_s = source length.

With the volumetric flow rate and oil mass, depletion rate constants were calculated as

$$\lambda_s = \frac{Q}{m_o \left(K_i^{o-w} / \rho^o \right)}, \quad (4-12)$$

where

Q = volumetric flow rate of water [cm³/day]

m_o = oil mass in source zone [g].

4.4.3.3 Modeling Results and Analysis

Theoretical equilibrium aqueous concentration values (C_0) for each hydrocarbon component (Table 4-2) were determined via equation 4-12 from component characteristics as given in Table 3-3. Values for λ_s were calculated with equations

The one-dimensional pulse injection model was fitted to the collected methanol data, yielding values for Pe of 7.5 and 9 for port 1 and port 2, respectively.

The plume transport model was fitted to hydrocarbon concentrations measured downstream of the NAPL source, yielding values for the parameters C_0 , Da_s and λ_s at ports 1 and 2 for each hydrocarbon component (Table 4-3). Values of Pe of 7.5 and 9 for port 1 and port 2, respectively, were used based on the values for methanol.

Table 4-4. Theoretical calculated parameters

	K_i^{o-w}	$C_{0,eq}$ [mg/L]	Q [cm ³ /day]	m_o [g]	λ_s [day ⁻¹]
Benzene	300	53.7	49.2	21.6	0.0067
Toluene	1223	35.2	49.2	21.6	0.0016
m-Xylene	2990	20.0	49.2	21.6	0.0004
1,2,4-TMB	9617	15.7	49.2	21.6	0.0001

Table 4-5. Model fitted parameters

	Port 1			Port 2		
	C_0 [mg/L]	λ_s [day ⁻¹]	Da_s	C_0 [mg/L]	λ_s [day ⁻¹]	Da_s
Benzene	50	0.060	0.0150	46	0.044	0.0400
Toluene	43	0.012	0.0060	43	0.014	0.0130
m-Xylene	30	0.003	0.0016	30	0.004	0.0035
1,2,4-TMB	28	0.001	0.0005	28	0.001	0.0011

Values for C_0 generated by the model were comparable to the values predicted from the physical properties of the hydrocarbon components. This similarity suggested that equilibrium dissolution initially occurred for flow passing through the source.

However, the theoretical λ_s values were significantly less than those fitted from the model for each hydrocarbon component. This indicated that the source depleted more rapidly than would be expected for water flow in equilibrium contact with NAPL throughout the source zone. The quicker depletion rate suggested that water contact with the NAPL was limited to a small fraction of the source, indicating that flow bypassing occurred for the remaining NAPL for which dissolution was mass transfer limited.

A time lag of 9 days was used for modeling the hydrocarbon breakthrough curves for ports 1 and 2. Hydrocarbons would have been expected to break through at the same time as the methanol if groundwater was in contact with the NAPL immediately after the release. However, this was not observed. This lag in hydrocarbon breakthrough indicates that the pore water passing by ports 1 and 2 initially after the release was not in contact with the NAPL. Therefore, it is likely that the lag was the result of initial depression of the capillary fringe due to high methanol concentrations followed by an increase after methanol was depleted from the source.

CHAPTER 5: SOURCE MODELING

Solutions to the advection-diffusion (A-D) equation can be derived for various continuous sources: the point source, the Gaussian source and the finite line source. The solutions can be used to predict downstream pore-water concentrations emanating from a residual NAPL source for sources of finite size. These solutions are compared with the one-dimensional (infinite line source) transport model used in Chapter 4 in the analysis of the pore water data.

5.1 Advection-Diffusion Equation

The general 3-dimensional A-D equation is

$$\left[D_x \frac{\partial^2 C}{\partial x^2} + D_y \frac{\partial^2 C}{\partial y^2} + D_z \frac{\partial^2 C}{\partial z^2} \right] - \left[v_x \frac{\partial C}{\partial x} + v_y \frac{\partial C}{\partial y} + v_z \frac{\partial C}{\partial z} \right] = \frac{\partial C}{\partial t}, \quad (5-1)$$

which can be simplified to two dimensions with a uniform flow field as

$$D_L \frac{\partial^2 C}{\partial x^2} + D_T \frac{\partial^2 C}{\partial y^2} - v_x \frac{\partial C}{\partial x} = \frac{\partial C}{\partial t}. \quad (5-2)$$

These general equations carry the following assumptions: a conservative substance, a homogeneous medium, and a fully saturated system. The conditions approximate those of solutes dissolved in an aqueous plume emanating from a fuel release in the saturated zone with continuous flow as in the 2-D experiments described above.

5.2 Continuous Source Parameters

The effective diffusion coefficient is defined (Fetter 1993) as

$$D^* = \omega D_d, \quad (5-3)$$

where

D^* = effective diffusion coefficient [cm²/day]

ω = coefficient related to tortuosity

D_d = diffusion coefficient [cm²/s].

Using this quantity, the longitudinal and transverse dispersion coefficients are given as

$$D_L = \alpha_L v_i + D^* \quad (5-4)$$

and

$$D_T = \alpha_T v_i + D^* , \quad (5-5)$$

where

D_L = longitudinal hydrodynamic dispersion coefficient

D_T = transverse hydrodynamic dispersion coefficient

α_i = dynamic dispersivity in the i direction

v_i = average linear velocity in the i direction.

The parameters used in the A-D equations (Table 5-1) were selected to mimic the conditions of the methanol-blended fuel release experiments.

Table 5-1. Continuous source parameters

Tortuosity Coefficient	ω	=	0.7
Linear Velocity	v_i	=	24 cm/day
Diffusion Coefficient (Benzene), 25°C	D_d	=	1.02×10^{-5} cm ² /s
Effective Diffusion Coefficient	D^*	=	0.617 cm ² /day
Longitudinal Dispersivity	α_L	=	0.3 cm
Transverse Dispersivity	α_T	=	0.1 cm
Longitudinal Dispersion Coefficient	D_L	=	0.782×10^{-3} m ² /day
Transverse Dispersion Coefficient	D_T	=	0.302×10^{-3} m ² /day

5.3 Continuous Source Solutions

5.3.1 Point Source Solutions

Fetter (1993) presented solutions for a continuous point source injection into a uniform two-dimensional flow field. The transient point source solution for concentration as a function of position and time is

$$C(x, y, t) = \frac{C_0(Q/b)}{4\pi\sqrt{D_L D_T}} \int_{\theta=0}^{\theta=t} \exp \left[-\frac{(x-v_x\theta)^2}{4D_L\theta} - \frac{y^2}{4D_T\theta} \right] \frac{d\theta}{\theta}, \quad (5-6)$$

where

C_0 = injection solute concentration [mg/L]

Q = rate of contaminant injection, and

b = aquifer thickness over which contaminant source is injected [m].

The steady-state point source solution is

$$C(x, y) = \frac{C_0(Q/b)}{2\pi\sqrt{D_L D_T}} \exp \left[\frac{v_x x}{2D_L} \right] K_0 \left[\left(\frac{v_x^2}{4D_L} \left(\frac{x^2}{D_L} + \frac{y^2}{D_T} \right) \right)^{1/2} \right], \quad (5-7)$$

where

K_0 = modified Bessell function of the second kind and zero order.

Concentration profiles were calculated from the point source solutions using parameters consistent with the methanol fuel experiments (Table 5-2).

Table 5-2. Point source solution parameters

Contaminant Injection Rate	Q	=	0.25 mL/min
Source Thickness	b	=	1.5 cm

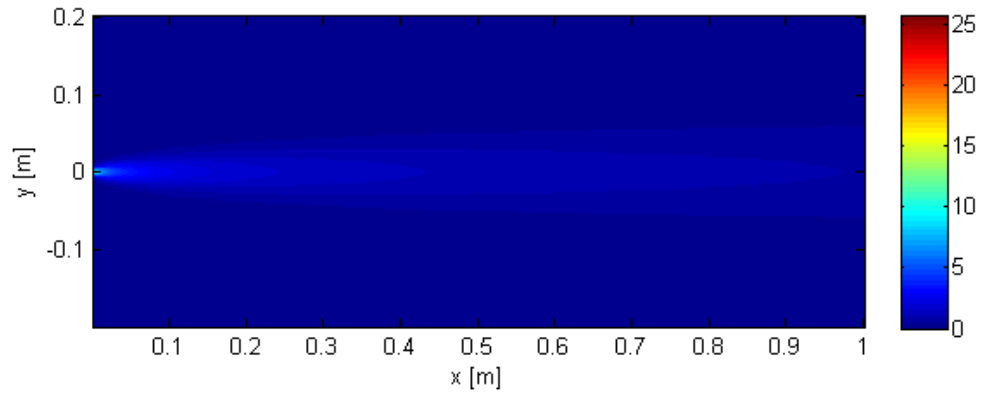


Figure 5-1. Transient point source solution (Eq. 5-6) dimensionless concentrations C/C_0 after one week.

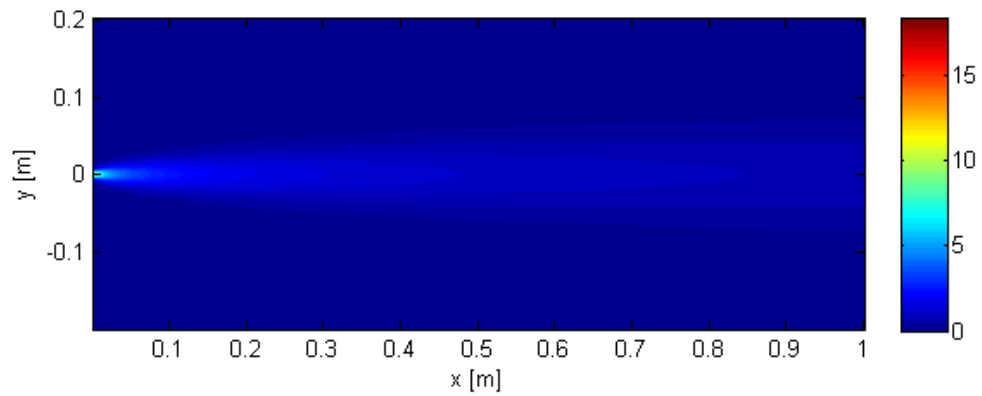


Figure 5-2. Steady-state point source solution (Eq. 5-7) dimensionless concentrations C/C_0 .

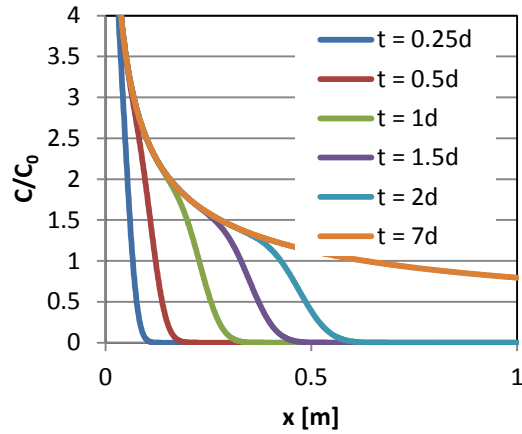


Figure 5-3. Dimensionless centerline concentrations downstream of a point source at various times (Eq. 5-6).

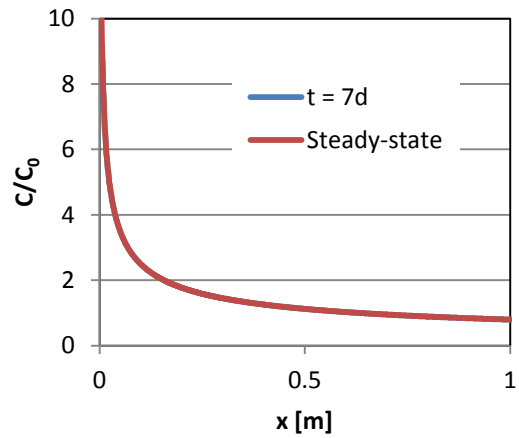


Figure 5-4. Dimensionless centerline concentrations downstream of a point source for transient ($t = 7$ days) and steady-state (Eq. 5-7) conditions.

At distances less than 0.63 m, the dimensionless centerline concentrations C/C_0 calculated from the point source solution are greater than 1. Approaching the source, concentrations approach infinity. These high concentrations are due to the source representation in the model as a single point through which a large amount of solute is injected. The transient point source solution approaches the steady-state centerline concentration profile after 7 days.

5.3.2 Gaussian Source Solution

The Gaussian source plume model in two dimensions (Charbeneau 2000) gives the transient concentration

$$C(X, Y, T) = X \int_{\omega=0}^{\omega=T} \frac{\exp\left(-\frac{X^2}{4\omega} - \frac{Y^2}{2 + 4D\omega} + \frac{X}{2} - \frac{1 + 4\Lambda}{4}\omega\right)}{\sqrt{4\pi\omega^3(1 + D\omega)}} d\omega \quad (5-8)$$

for

$$X = \frac{v'x}{D_{L'}}, \quad (5-9)$$

$$Y = \frac{y}{\sigma}, \quad (5-10)$$

$$T = \frac{v'^2 t}{D_{L'}}, \quad (5-11)$$

$$\Lambda = \frac{\lambda^* D_{L'}}{v'^2}, \quad (5-12)$$

$$D = \frac{D_{L'} D_{T'}}{\sigma^2 v'^2}, \text{ and} \quad (5-13)$$

$$C = \frac{c}{c_0}, \quad (5-14)$$

where

σ = standard deviation for the Gaussian source concentration distribution [m]

λ^* = effective decay coefficient [day^{-1}]

v' = retarded velocity [m/day]

$D_{L'}$ = retarded longitudinal dispersion [m^2/day]

$D_{T'}$ = retarded transverse dispersion [m^2/day].

Retarded velocity and dispersion parameters are calculated as

$$v' = \frac{v}{R}, \quad (5-15)$$

$$D_L' = \frac{D_L}{R}, \text{ and} \quad (5-16)$$

$$D_T' = \frac{D_T}{R}, \quad (5-17)$$

where

R = retardation coefficient.

Parameter values analogous to the methanol fuel experiments (Table 5-3) were used in calculating the solution.

Table 5-3. Gaussian source solution parameters

Standard Deviation	σ	=	0.025 m
Effective Decay Coefficient	λ^*	=	0 day ⁻¹
Retardation Factor	R	=	1
Retarded Velocity	v'	=	24 cm/day
Retarded Longitudinal Dispersion	D_L'	=	0.782 x 10 ⁻³ m ² /day
Retarded Transverse Dispersion	D_T'	=	0.302 x 10 ⁻³ m ² /day

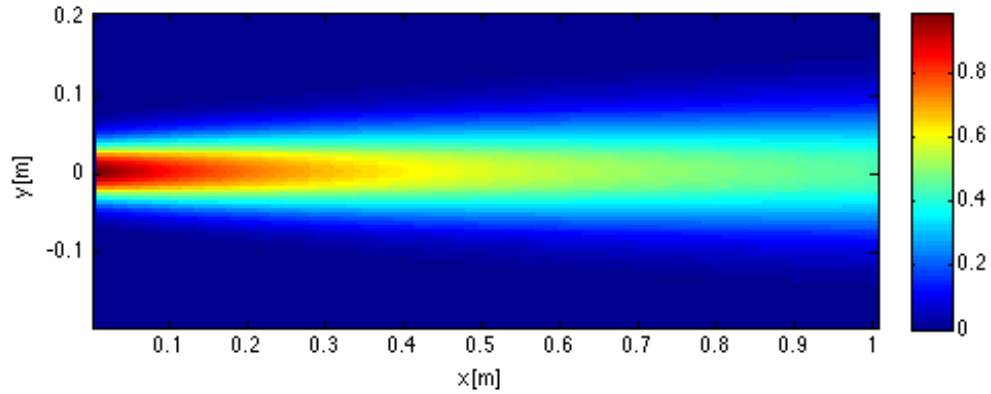


Figure 5-5. Dimensionless concentrations C/C_0 downstream of a continuous Gaussian source ($\sigma = 2.5$ cm) after one week.

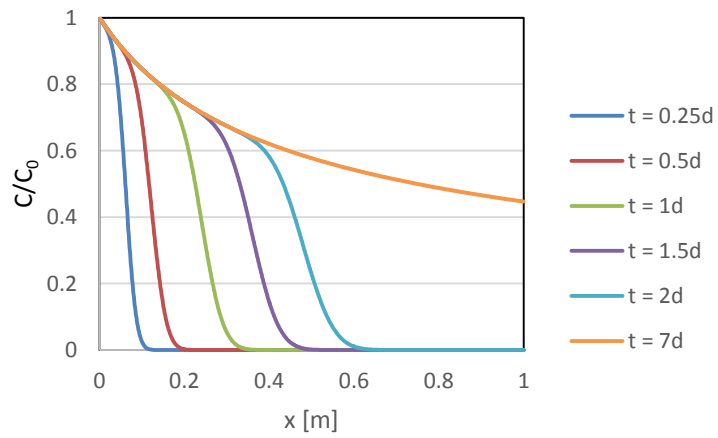


Figure 5-6. Dimensionless centerline concentration profiles downstream of a continuous Gaussian source ($\sigma = 2.5$ cm) at various times.

5.3.3 Finite Line Source Solution

The steady-state finite line source solution in two dimensions (Brooks 1960) is

$$C(x, y) = \frac{c_0}{2\sqrt{\pi D_T t}} \int_{-b/2}^{b/2} \exp\left(-\frac{(y-y')^2}{4D_T t}\right) dy', \quad (5-18)$$

where

$$t = \frac{x}{v} \quad (5-19)$$

and

$b =$ source width [m]

with the assumption of negligible longitudinal mixing. The source width b was set at 10 cm for the model calculations.

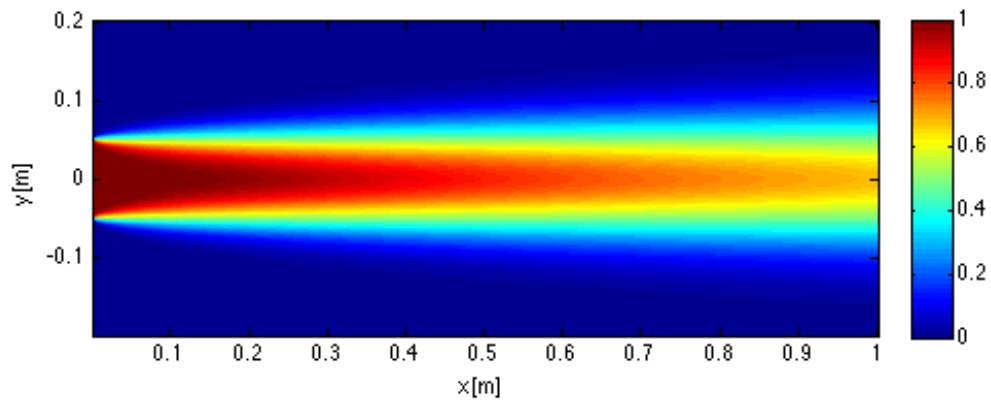


Figure 5-7. Steady-state dimensionless concentrations C/C_0 downstream of a finite line source of width $b = 10$ cm.

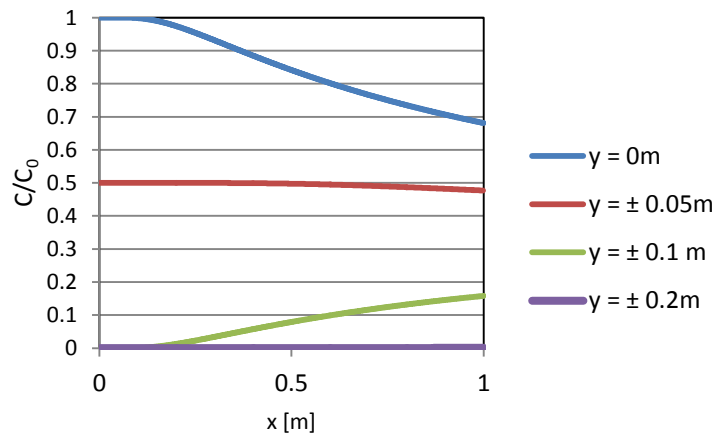


Figure 5-8. Steady-state concentration profiles downstream of a finite line source of width $b = 10$ cm.

5.3.4 Comparison of Continuous Source Models

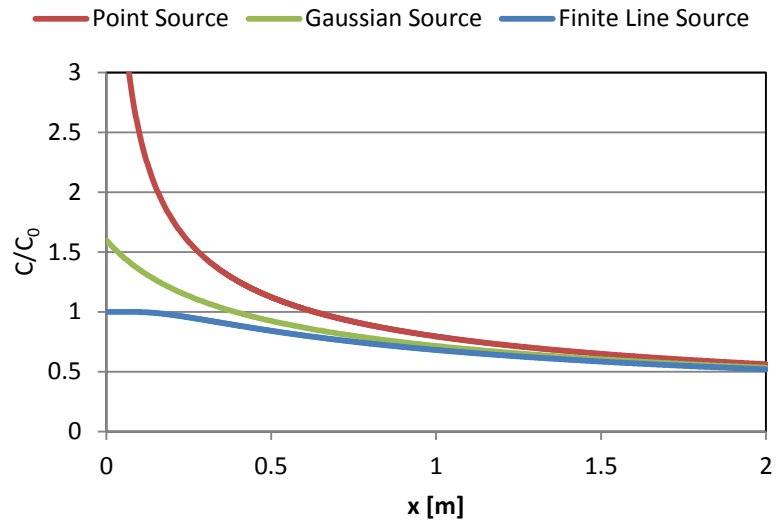


Figure 5-9. Steady-state centerline concentration profiles for Gaussian, finite line, and point sources.

Given the source width and standard deviation used for the finite line and Gaussian sources, respectively, Gaussian source model concentrations were multiplied by a factor of $4/(2\pi)^{0.5} = 1.596$ in comparing the three source models to yield the same average source strength as the finite line source. With this adjustment of the Gaussian source concentrations, centerline concentrations generated by the three source models (point, Gaussian and finite line) converged as distance from the source increased. At 2 m from the source, concentrations from the three sources were closely matched.

In the immediate vicinity of the source, the point and Gaussian source models generated concentrations much greater than the concentration injected. This behavior was most pronounced in the point source model, which generated infinite concentrations at the source. Unlike the point and Gaussian source models, however, concentrations predicted by the finite line source remained close to the injected concentration for a short distance from the source before beginning to decline.

Though the three source models generate comparable concentrations at larger distances from the source, the point and Gaussian source models are not appropriate for short distances from the source as they do not generate reasonable concentrations at these distances. Therefore, at small distances downstream of the source (relative to source thickness), the finite line source model should be used. Further, the results for the finite line source also show that the use of the infinite line source model (Equation 4-6) was appropriate for analysis of the pore water data presented in Chapter 4.

CHAPTER 6: CONCLUSIONS AND FUTURE WORK

6.1 Blended Fuel Releases

The behavior of the methanol- and ethanol-blended fuels was notably impacted by the volume percent of alcohol in the fuels. Over the course of the weeklong experiments, several common characteristics were observed among the methanol and ethanol blends: spreading of the NAPL source zone, redistribution of NAPL within the source zone, phase separation of the alcohol and depression of the capillary fringe.

After the fuel injection and initial generation of the NAPL source, the area of the source zone increased with time. This expansion of the source area increased with increasing alcohol content. The final spill areas measured one week after injection were higher for the ethanol blends than for the equivalent methanol blends at each volume % of alcohol tested. Correspondingly, final saturation measured one week after injection decreased with increasing alcohol content in the fuels.

As the areal extent of the NAPL sources increased, the NAPL within the source zones was redistributed. For the high alcohol-content blends (85 % v/v alcohol), high saturations of NAPL were present at the edge of the source zone, surrounding a lower-saturation center. With the lower ethanol-content blends (E15, E25 and E50), a low saturation middle region was formed between higher-saturation regions of the source above and below. A similar lower-saturation middle region was observed only in the M50 injection, however.

Further, these NAPL distributions may also impact the level and duration of pore-water concentrations emanating from a NAPL source. The low overall source zone saturation for the high alcohol content fuels (85% v/v alcohol) indicated good flow

through the source and thus initially potentially greater, but shorter-lived BTX pore water concentrations, while the higher overall saturation of the low alcohol-content fuels indicated reduced flow through the source zone and potentially lower, longer-lived BTX concentrations in the pore-water downstream of the source.

Because of the alcohols' preference to partition into the aqueous phase, surface tension of the aqueous phase was reduced, leading to depression of the capillary fringe. This capillary fringe depression was observed in all of the injected blends with greater depression occurring with the higher alcohol-content fuels. Some capillary fringe recovery was observed over the experiments' duration for the higher alcohol content fuels.

6.2 Pore Water Impacts

The larger 75-mL M15 release behaved similarly to the smaller 30-mL M15 release based on the visualization data. In the pore-water concentration data collected, however, a lag was observed in the breakthrough of hydrocarbons at the sampling ports directly downstream of the injection, likely due to temporary initial capillary fringe depression as a result of the large quantity of methanol present. Fitting the hydrocarbon pore-water concentration data to a plume transport model yielded characteristic parameter values for the release. Theoretical equilibrium aqueous concentrations compared well with those inferred from the experiments. However, experimental source depletion rates were much greater than expected based on theoretical calculations, indicating that flow bypassed a significant fraction of the remaining NAPL source.

6.3 Source Modeling

Point, Gaussian and finite line sources were compared for conditions approximating those of the fuel release experiments. Concentration profiles generated by all three sources converged around 2 m from the source. However, only the finite line source was applicable at short distances from the source.

6.4 Recommendations for Future Work

The work presented here illustrates the behavior of methanol- and ethanol-blended fuels of varying alcohol content. It may be extended through further investigation of pore-water hydrocarbon concentrations downstream of the source as well as investigations of the release characteristics of other fuel oxygenates.

(1) Downstream Pore-water Concentrations

The pore-water measurements taken from the 75-mL M15 release demonstrated a lag in the breakthrough of the hydrocarbon components, most likely due to rebound in the height of the capillary zone after methanol was depleted. By collecting pore-water concentration measurements for fuel blend releases with higher methanol contents, this behavior may be further elucidated and pore-water impacts for varying blends can be quantified. In addition, measurements of the effect of bypassing of NAPL on longer-term hydrocarbon (BTX and TMB) pore-water impacts for fuel blends of higher alcohol contents are needed.

(2) Other Fuel Oxygenates

With increasing demand for oxygenated fuels worldwide, interest in other oxygenates will increase. These include other alcohols such as isobutanol. Understanding

the environmental impacts of these alternative oxygenates will be important for management of spills associated with these alternative fuels.

REFERENCES

- Barker, J. F., C. E. Hubbard, and L. A. Lemon. "The Influence of Methanol and MTBE on the Fate and Persistence of Monoaromatic Hydrocarbons in Groundwater," *Proceedings of the National Water Well Association/American Petroleum Institute Conference: Petroleum Hydrocarbons and Organic Chemicals in Groundwater*, Houston, TX, Oct. 31-Nov. 2, 1990, pp. 113-127.
- Barker, J. F., C. E. Hubbard, L. A. Lemon, and K. A. Vooro. (1992). "The Influence of Methanol in Gasoline Fuels on the Formation of Dissolved Plumes, and on the Fate and Natural Remediation of Methanol and BTEX Dissolved in Groundwater." Hydrocarbon Contaminated Soils and Groundwater, Vol 2. Boca Raton, Lewis Publishers Inc: 103-113.
- Bromberg, L. and Cheng, W.K. "Methanol as an Alternative Transportation Fuel in the U.S.: Options for Sustainable and/or Energy-Secure Transportation," Massachusetts Institute of Technology, November 2010.
- Brooks, N.H. (1960). "Diffusion of Sewage Effluent in an Ocean Current." *Proceedings of the First International Conference on Waste Disposal in the Marine Environment*, 1st. pp. 246-267. Pergamon, Oxford.
- Cápiro, N. L., Stafford, B. P., Rixey, W. G., Bedient, P. B., & Alvarez, P. J. J. (2007). "Fuel-grade Ethanol Transport and Impacts to Groundwater in a Pilot-scale Aquifer Tank." *Water Research*, 41(3), 656-664.
- Charbeneau, Randall J. (2000), Groundwater Hydraulics and Pollutant Transport, Prentice Hall, Upper Saddle River, NJ.

- Donaldson, C.R., Barker, J.F., & Chatzis, I. (1993). "Oxygenated Fuel (M-85) Behavior in the Subsurface -- A Laboratory Scale Investigation." *Proceedings of the Conference on Petroleum Hydrocarbons and Inorganic Chemicals in Groundwater*, November, Houston, TX, Ground Water Publishing Company, Dublin, Ohio.
- Fetter, C.W. (1993), Contaminant Hydrogeology, Macmillan Pub. Co., New York, NY.
- Freitas, J. G., & Barker, J. F. (2011). "Oxygenated Gasoline Release in the Unsaturated Zone - Part 1: Source Zone Behavior." *Journal of Contaminant Hydrology*, 126(3-4), 153-166.
- Freitas, J. G., & Barker, J. F. (2013). "Denatured Ethanol Release into Gasoline Residuals, Part 1: Source Behaviour." *Journal of Contaminant Hydrology*, 148, 67-78.
- Freitas, J. G., Doulatyari, B., Molson, J. W., & Barker, J. F. (2011). "Oxygenated Gasoline Release in the Unsaturated Zone, Part 2: Downgradient Transport of Ethanol and Hydrocarbons." *Journal of Contaminant Hydrology*, 125(1-4), 70-85.
- Gaffney, J. S., Streit, G. E., Spall, W. D., & Hall, J. H. (1987). "Beyond Acid Rain." *Environmental Science and Technology*, 21(6), 519-524.
- Garg, S., & Rixey, W. G. (1999). "The Dissolution of Benzene, Toluene, m-Xylene and Naphthalene from a Residually Trapped Non-aqueous Phase Liquid Under Mass Transfer Limited Conditions." *Journal of Contaminant Hydrology*, 36(3-4), 313-331.

- Hao, L., & Leaist, D. G. (1996). "Binary Mutual Diffusion Coefficients of Aqueous Alcohols. Methanol to 1-Heptanol." *Journal of Chemical and Engineering Data*, 41(2), 210-213.
- He, X., Stafford, B. P., & Rixey, W. G. (2011). "Ethanol-enhanced Dissolution of a Residually Trapped Synthetic Gasoline Source." *Ground Water Monitoring and Remediation*, 31(3), 61-68.
- Heermann, S. E., & Powers, S. E. (1998). "Modeling the Partitioning of BTEX in Water-reformulated Gasoline Systems Containing Ethanol." *Journal of Contaminant Hydrology*, 34(4), 315-341.
- ITRC (Interstate Technology & Regulatory Council). 2011. Biofuels: Release Prevention, Environmental Behavior, and Remediation. BIOFUELS-1. Washington, D.C.: Interstate Technology & Regulatory Council, Biofuels Team. www.itrcweb.org.
- Lee, K. Y. (2008). "Phase Partitioning Modeling of Ethanol, Isopropanol, and Methanol with BTEX Compounds in Water." *Environmental Pollution*, 154(2), 320-329.
- Lee, K. Y., & Ha, D. T. (2012). "Viscosity Variations of Three-component Mixtures Comprising an Alcohol, Various Common Groundwater Contaminants, and Water." *Environmental Engineering Science*, 29(1), 26-34.
- Lide, D.R., 2013. CRC Handbook of Chemistry and Physics. 95th edition, CRC Press, Inc., Boca Raton, FL.
- Mamonkina, I. (2011). "Physical-Model Simulations of Spills of Ethanol-Blended Fuels." M.S. Thesis, University of Houston, Houston, TX.

- McDowell, C. J., & Powers, S. E. (2003). "Mechanisms Affecting the Infiltration and Distribution of Ethanol-blended Gasoline in the Vadose Zone." *Environmental Science and Technology*, 37(9), 1803-1810.
- McDowell, C. J., Buscheck, T., & Powers, S. E. (2003). "Behavior of Gasoline Pools Following a Denatured Ethanol Spill." *Ground Water*, 41(6), 746-757.
- O'Neil, M.J., (Ed.). (2006). The Merck Index: An Encyclopedia of Chemicals, Drugs, and Biologicals (14th ed.). NJ: Merck.
- Oliviera, I. B., Demond, A. H., & Salehzadeh, A. (1996). "Packing of Sands for the Production of Homogeneous Porous Media." *Soil Science Society of America Journal*, 60(1), 49-53.
- Poulsen, M., Lemon, L., & Barker, J. F. (1992). "Dissolution of Monoaromatic Hydrocarbons into Groundwater from Gasoline-oxygenate Mixtures." *Environmental Science and Technology*, 26(12), 2483-2489.
- Reed, T. B., & Lerner, R. M. (1973). "Methanol: A Versatile Fuel for Immediate Use." *Science*, 182(4119), 1299-1304.
- Rixey, W. G. and I. J. Dortch (1992). "Effects of Oxygenated Fuels on Groundwater Contamination: Equilibria and Transport Considerations." Hydrocarbon Contaminated Soils and Groundwater, Vol 2. Boca Raton, Lewis Publishers Inc: 115-136.
- Rixey, W. G., He, X., & Stafford, B. P. (2005). "The Impact of Gasohol and Fuel-grade Ethanol on BTX and Other Hydrocarbons in Ground Water: Effect on Concentrations near a Source." *API Soil and Groundwater Research Bulletin No.* 23.

- Sangster, J. (1989). "Octanol-Water Partition Coefficients of Simple Organic Compounds." *J. Phys. Chem. Ref. Data*, 18(3), 1111-1227.
- Stafford, B. P. (2007). "Impacts to Ground Water from Releases of Fuel Grade Ethanol: Source Behavior." Ph.D. Dissertation, University of Houston, Houston, TX.
- Stafford, B. P., Cápiro, N. L., Alvarez, P. J. J., & Rixey, W. G. (2009). "Pore Water Characteristics Following a Release of Neat Ethanol onto Pre-existing NAPL." *Ground Water Monitoring and Remediation*, 29(3), 93-104.
- U.S. Department of Agriculture, Agricultural Marketing Service. "Ethanol Transportation Backgrounder," September 2007. Web. <http://dx.doi.org/10.9752/TS029.09-2007>
- US EPA, "Oxygenates in Water: Critical Information and Research Needs." EPA/600/R/98/048, December 1998.
- Yang, C., & Jackson, R. B. (2012). "China's Growing Methanol Economy and its Implications for Energy and the Environment." *Energy Policy*, 41, 878-884.
- Zhang, Y. (2014). "Subsurface Source Generation and Transport from Spills of Alcohol-Blended Fuels." Ph.D. Dissertation, University of Houston, Houston, TX.

**APPENDIX A: METHANOL RELEASE VISUALIZATION – ADDITIONAL
DATA**

Figure A.1. Visualization of 30-mL M15 release in the capillary zone at various times. **70**

Figure A.2. Visualization of 30-mL M25 release in the capillary zone at various times. **71**

Figure A.3. Visualization of 30-mL M50 release in the capillary zone at various times. **72**

Figure A.4. Visualization of 30-mL M85 release in the capillary zone at various times. **73**

Figure A.5. Visualization of 75-mL M15 release in the capillary zone at various times. **74**

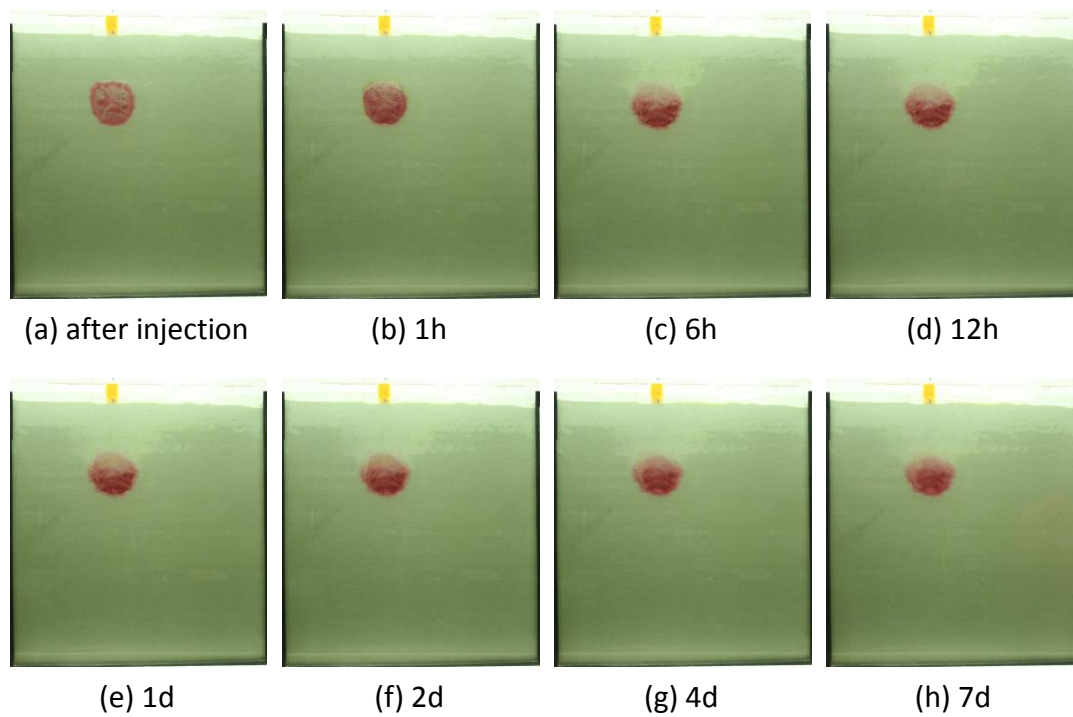


Figure A.1. Visualization of 30-mL M15 release in the capillary zone at various times.

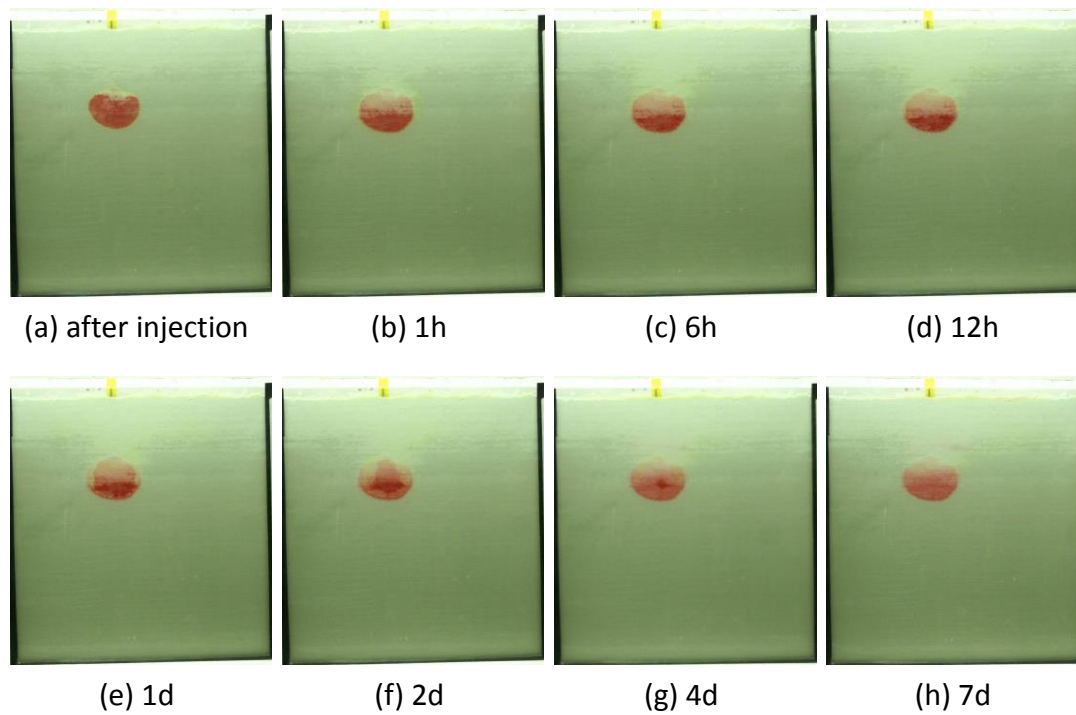


Figure A.2. Visualization of 30-mL M25 release in the capillary zone at various times.

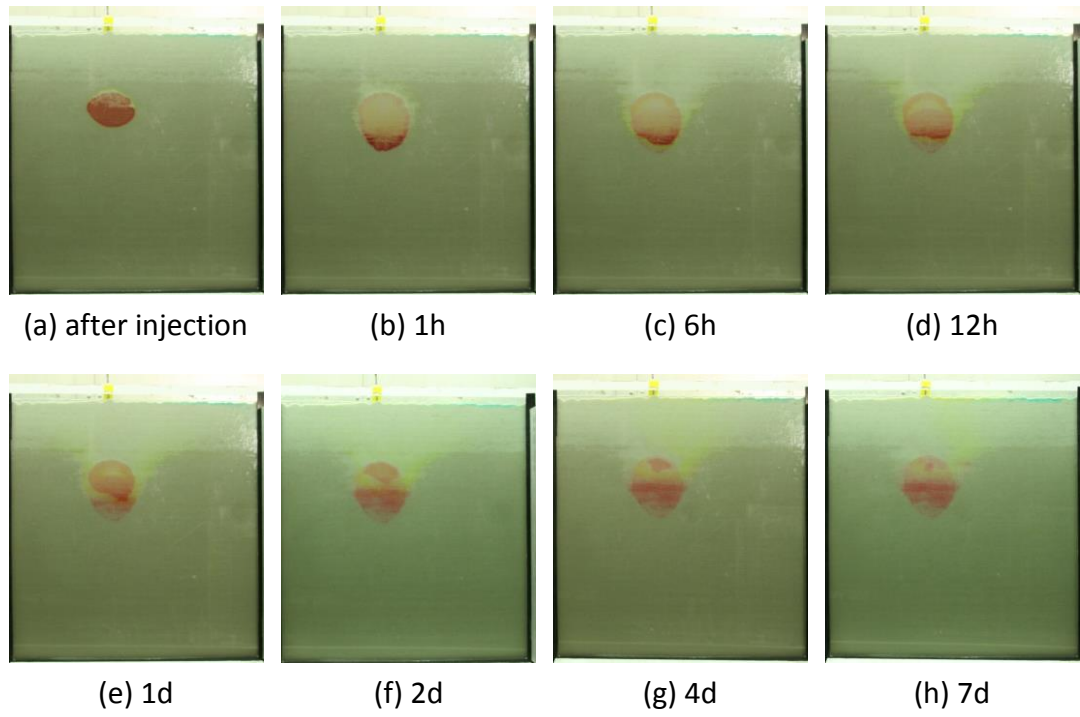


Figure A.3. Visualization of 30-mL M50 release in the capillary zone at various times.

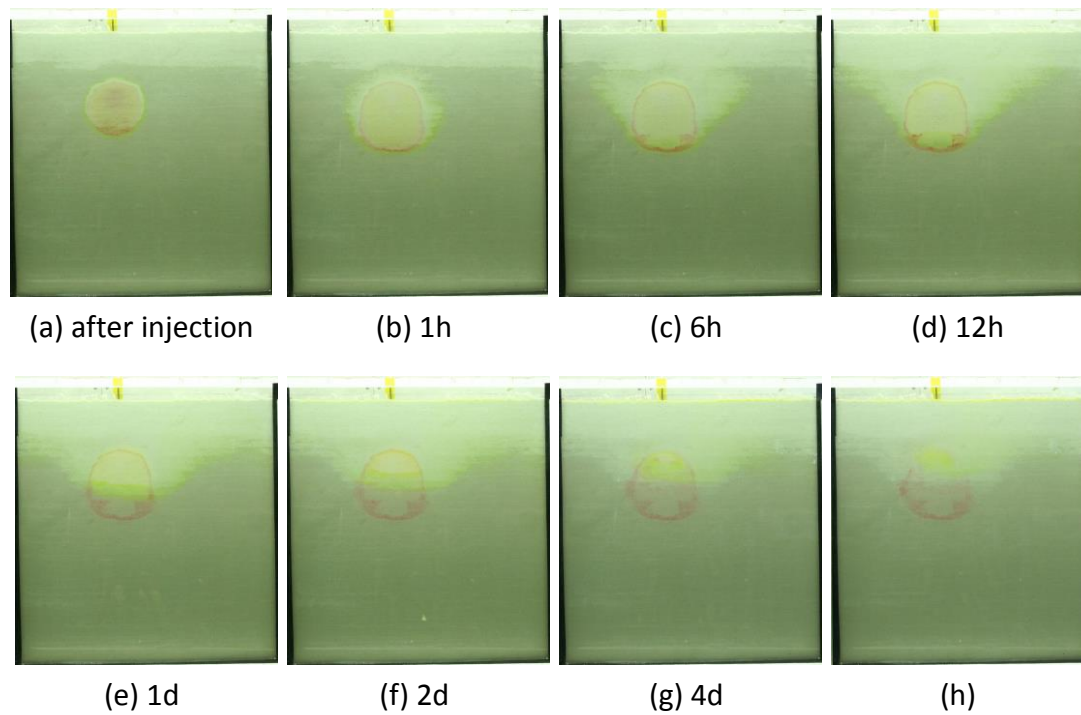


Figure A.4. Visualization of 30-mL M85 release in the capillary zone at various times.

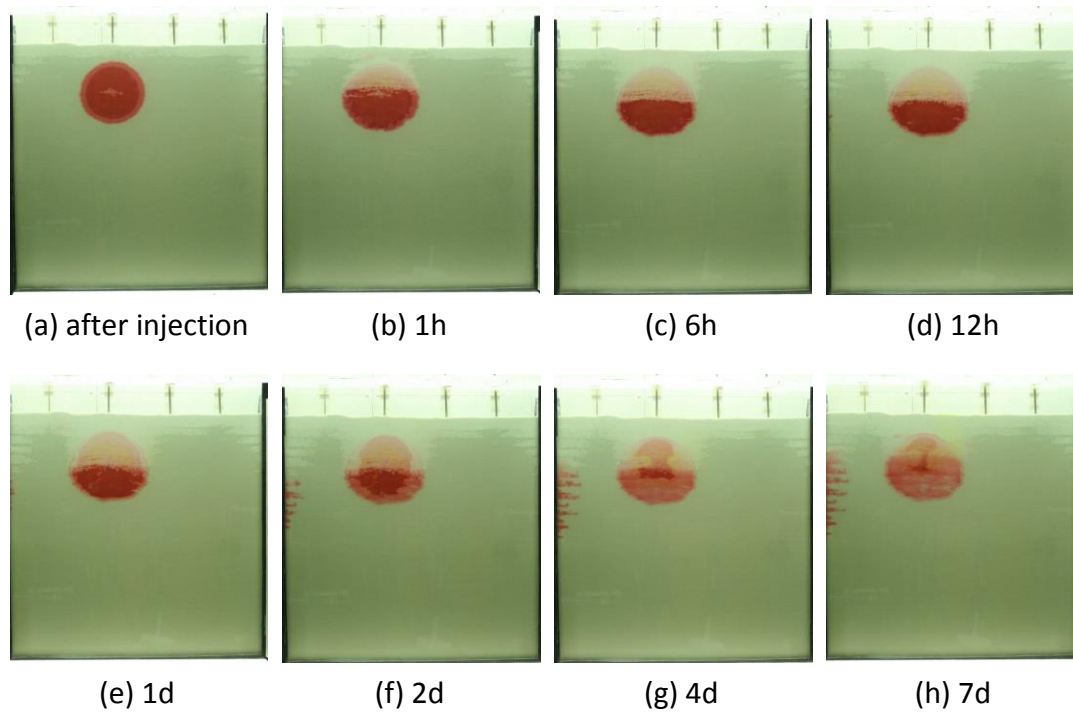


Figure A.5. Visualization of 75-mL M15 release in the capillary zone at various times.

APPENDIX B: 75-ML M15 RELEASE POREWATER MEASUREMENTS

Table B.1. Porewater measurements from Port 1 (Figure 4-14). **76**

Table B.2. Porewater measurements from Port 2 (Figure 4-15). **77**

Table B.3. Porewater measurements from Port 3 (Figure 4-16). **78**

Table B.1. Porewater measurements from Port 1 (Figure 4-14).

Sample #	Day	Concentration [mg/L]				
		MeOH	Benzene	Toluene	Xylene	1,2,4-TMB
1	0.00	94.252				
2	0.51	1538.703				
3	1.80	2100.220				
4	2.80	1715.512				
5	3.71	532.239				
6	4.76	164.461				
7	6.05					
8	6.72	77.997				
9	7.70	66.162				
10	9.04	13.258	8.669	11.449	4.004	
11	10.73	40.173	45.027	41.874	32.885	29.775
12	11.89	0.000	27.411	28.772	26.828	23.438
13	13.05	51.005				
14	13.70					
15	14.69		38.182	41.836	30.468	28.865
16	17.84					
17	18.79					
18	19.73		27.900	35.627	25.714	23.241
19	20.81					
20	21.81					
21	24.69		23.642	38.930	27.974	23.536
22	28.67		10.932	24.351	23.065	23.256
23	31.72					
24	32.77					
25	33.71		15.450	37.010	35.080	32.685
26	34.75					
27	38.78			21.812	24.397	27.340
28	42.73		3.834	33.580	34.580	36.867
29	45.81		5.724	34.041	36.882	41.762
30	47.77			21.760	16.739	17.757

Table B.2. Porewater measurements from Port 2 (Figure 4-15).

Sample #	Day	Concentration [mg/L]				
		MeOH	Benzene	Toluene	Xylene	1,2,4-TMB
1	0.00	53.264				
2	0.51	13.696				
3	1.80	1808.379				
4	2.80	2981.568				
5	3.71	3071.013				
6	4.76	1954.823				
7	6.05	1658.885				
8	6.72	492.586				
9	7.70	350.131				
10	9.04	113.755	12.057			
11	10.73	56.276	33.395	30.573	33.781	23.444
12	11.89	0.000	39.972	38.213	27.870	27.216
13	13.05	67.914				
14	13.70					
15	14.69		23.293	25.387	19.499	21.385
16	17.84					
17	18.79					
18	19.73		38.213	44.870	32.068	30.220
19	20.81					
20	21.81					
21	24.69		29.583	46.014	35.172	35.046
22	28.67		19.825	40.097	33.562	35.610
23	31.72					
24	32.77					
25	33.71		11.004	24.489	22.753	25.976
26	34.75					
27	38.78		16.910	37.749	23.287	22.781
28	42.73		13.753	31.852	30.244	33.674
29	45.81					11.874
30	47.77					

Table B.3. Porewater measurements from Port 3 (Figure 4-16).

Sample #	Day	Concentration [mg/L]				
		MeOH	Benzene	Toluene	Xylene	1,2,4-TMB
1	0.00	55.966				
2	0.51	14.752				
3	1.80	34.597				
4	2.80	68.233				
5	3.71	59.026				
6	4.76	0.000				
7	6.05	41.994				
8	6.72	43.932				
9	7.70	56.180				
10	9.04	24.357				
11	10.73	23.223				
12	11.89	8.942	11.020	11.928		
13	13.05	40.135				
14	13.70					
15	14.69		12.626	16.907	14.072	15.347
16	17.84					
17	18.79					
18	19.73		12.893	18.581	12.831	11.969
19	20.81					
20	21.81					
21	24.69			15.746	12.788	12.327
22	28.67					
23	31.72					
24	32.77					
25	33.71					10.235
26	34.75					
27	38.78					
28	42.73					
29	45.81					
30	47.77					

APPENDIX C: CAPILLARY PRESSURE-WATER SATURATION MEASUREMENTS

Figure C.1. Pressure head-saturation profile for Ottawa sand using a saturated packing

method..... **80**

The capillary pressure-water saturation curve was measured in the larger (50 cm x 55 cm x 1.5 cm) cell. The curve is given in Figure C.1.

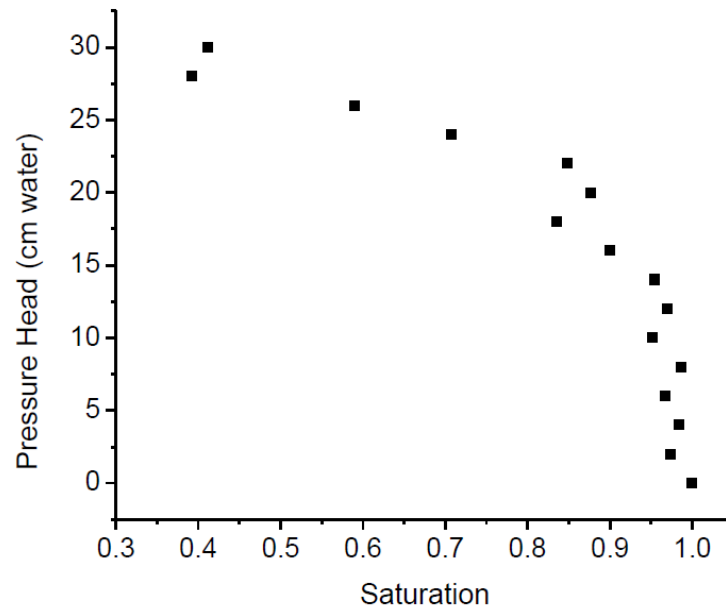


Figure C.1. Pressure head-saturation profile for Ottawa sand using a saturated packing method (Zhang 2014).